Frontiers in Experimental Fluid Mechanics
ed M. Gad-el-Hak, Springer, pp. 159-209, 1989

The turbulent boundary layer

K.R. Sreenivasan
Mason Laboratory, Yale University, New Haven, CT 06520

Abstract

This article is intended as a brief review of the dynamics of the turbulent boundary layer on a smooth flat wall. The emphasis is on physical arguments, and the contents offer the minimum ground that an advanced graduate student (who has some familiarity with the turbulence problem but not much with the boundary layer itself) ought to cover before embarking on his own research. But it is believed that the perspective is relatively new at places, and that the article is therefore of interest also the specialist. In section 2, classical notions are presented in a way that their strengths and weaknesses become transparent. This is followed in section 3 by a description of the structural features of the boundary layer. In both sections, some emphasis is given to the inner/outer interactions. The article ends with a discussion of a few open ended issues concerning the problem.

1. Introduction

A major practical reason for interest in turbulence is that it enhances mixing as well as transport of energy and matter; yet another is that it is responsible for a significant fraction of energy loss in internal and external flows. The understanding and control of turbulent boundary layers is an especially important problem technologically, and vast sums of money and effort have been spent on it. While a wealth of information now exists on the description of its various facets, a complete picture is yet to emerge, and our predictive and control capabilities based on first principles have remained far less adequate than practical needs would suggest.

We restrict attention largely to the fully-developed, two-dimensional turbulent boundary layer on a smooth, semi-infinite flat plate with no imposed pressure gradient, and the flow is assumed to be isothermal and incompressible. It is impossible to realize these conditions strictly in a laboratory, but close approximations have been produced. In practice, one encounters the turbulent boundary layer in the presence of three-dimensionalities, roughnesses, pressure gradients, curvature, heat transfer, compressibility, etc., some of which can have profound effects on the flow development. It is therefore useful to comment on the rationale for the excessive emphasis on this paradigmatic case. First, it is the simplest possible wall-bound turbulent flow: There is little hope of understanding other complex effects without the benefit of understanding this 'simple' case. Secondly, the properties of this special case are useful even in the presence of these complex effects – quantitatively if they are small and qualitatively otherwise.

The turbulent boundary layer possesses both 'universal' and case-specific properties; by definition, the universal aspects do not depend on the precise flow configuration (at least to a good approximation). Here, we focus attention on those aspects which make the turbulent boundary layer unique, and dwell less on the universal aspects.

Although the velocity field at each instant of time is believed to be governed exactly by the Navier-Stokes equations, their complexity makes it impossible to obtain the required information by directly solving them. (See section 4.1 for comments on the role of computer simulations.) Following Reynolds (1894), traditional turbulence studies reject the need for detailed instantaneous quantities, and proceed by decomposing the motion into its time mean (which is steady in the flow we are considering) and fluctuations around it; only the evolution of the mean and perhaps a first few moments of fluctuations are sought. We assume that the reader is familiar with the resulting closure problem (see, for example, Monin & Yaglom 1971), and the necessity for heuristic modeling. Alternatives to this so-called Reynolds decomposition have been proposed (e.g., Hussain 1983), especially motivated by the awareness that the coherent component of the turbulent motion needs to be explicitly built into a workable decomposition scheme, but their advantages are unclear at the moment. We shall follow tradition and adopt the Reynolds decomposition, keeping in mind that we must be willing to do away with this artifact under sufficiently compelling reasons.

The presence of the wall makes the turbulent boundary layer structure and dynamics profoundly different from those of unbounded (or 'free') shear flows. One of the primary differences is that there are in the turbulent boundary layer two distinct scales which are highly disparate at large Reynolds numbers. This makes true self-preservation impossible (except in the special case of the flow between two converging planes where the two scales can be forced to be proportional to each other at all Reynolds numbers). Unlike other fully turbulent flows in which *direct* viscous effects are negligible, they are *always* present in a small region near the wall of the turbulent boundary layer. The turbulent boundary layer can maintain large fluctuation levels close to the wall, successfully countering viscous and turbulent diffusion. The rate of turbulent energy production and dissipation peak very near the wall (figure 1). More than about a third of the total production and dissipation occurs within a distance from the wall which occupies no more than 2% of the flow thickness at typical laboratory Reynolds numbers (and an even smaller fraction at higher Reynolds numbers). This feature has no analog in free shear flows where the rate of turbulent energy production is the largest near the inflection point of the mean velocity profile, and is spread over the entire flow width; the energy dissipation is even more diffusely distributed (figure 2).

The wall-region of the boundary layer is thus perceived to serve an important function in maintaining the flow. As we shall see in section 2.1, the characteristic Reynolds number of this region is a small number of the order 30. Boundary layers at such low Reynolds numbers cannot be maintained 'turbulent' unless buffetted constantly by strong disturbances, and this necessary function can be expected to be served by the outer layer. At least in this sense, the maintenance of the turbulent boundary layer must owe itself to the interaction of the outer layer fluctuations with the near-wall region. Unfortunately, the precise way in which this interaction comes about is not fully understood: The complexity of the problem is such that there are differing views even on the kinematic description of the region near the wall, and on the very importance of the events occurring there. Section 2 provides a description based on classical notions (albeit with different emphasis at places), while section 3 summarizes the work on the boundary layer structure. In each of these sections, we first present descriptions of the wall-dominated region and the rest of the flow separately, and then examine the more complex problem of interactions; this latter is our emphasis

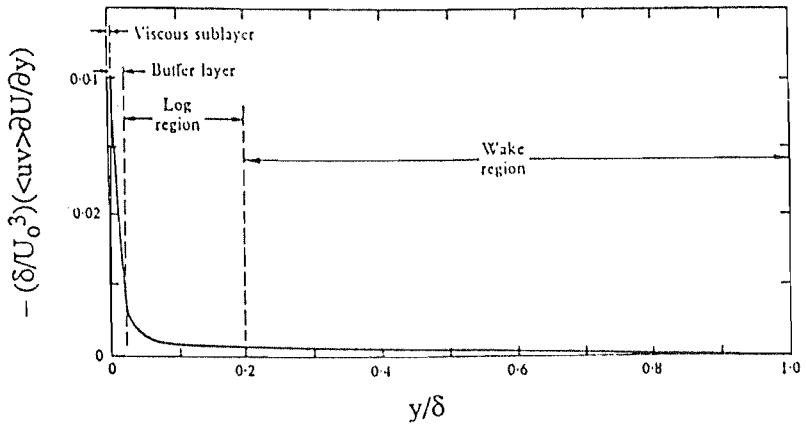

Figure 1. The turbulent energy production rate per unit volume is the product of the Reynolds stress $-\langle uv \rangle$ and the local velocity gradient $\partial U/\partial y$. This quantity normalized by the freestream velocity U_0 and the boundary layer thickness δ is plotted against y/δ, y being the distance measured from the wall normal to it. The curve, computed from Klebanoff's data, is adapted from Kline et al. (1967). The various regimes in the boundary layer will be explained at appropriate places in the text; so will other details.

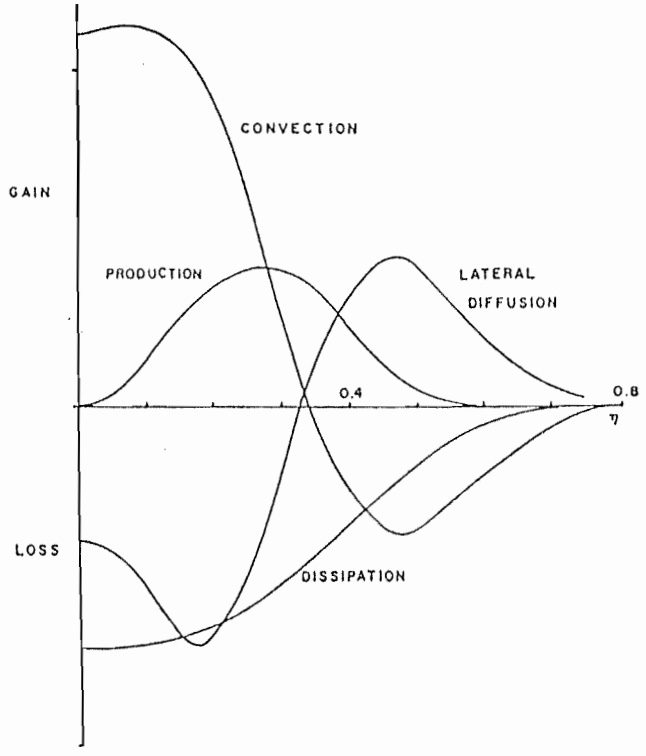

Figure 2. The turbulent energy balance in the plane wake behind a circular cylinder. Data of Townsend (1956). Here, η is the appropriately normalized distance in the direction of the largest shear. $\eta = 0$ is the wake centerline.

but, unfortunately, the task will have to be left unfinished at the present state of knowledge.

In the following section, we occasionally invoke similarities in the near-wall region between the boundary layer on the one hand, and pipe and channel flows on the other. The conditions in the outer region can be expected to be different in these two classes of flows because there is usually a turbulence-free uniform outer stream in the boundary layer while the flow in fully developed pipes and channels is turbulent right up to the geometric center. Furthermore, flow variables (except for the pressure) in fully-developed pipes and channels do not depend on the streamwise coordinate while such a dependence, even if a weak one, exists in the boundary layer.

2. The mean velocity and Reynolds stresses

In the Reynolds decomposition, the most important dynamical quantity affecting the mean motion is the so-called Reynolds or turbulent shear stress, $\tau = -\langle uv \rangle$, where u and v are the fluctuation velocities in the streamwise direction x and the direction y normal to the flat plate (see figure 3); the angular brackets indicate the time mean. (Here and elsewhere, unless explicitly remarked otherwise, capital letters indicate mean values and the corresponding lower case letters indicate fluctuations around the mean; for example, U and u are respectively the mean and fluctuating velocities in the direction x.) Since the Reynolds stress represents the significantly larger momentum transport accomplished by turbulence, modeling its behavior is one of the prime concerns of various prediction schemes.

A fully turbulent flow is characterized by the inequality that the turbulent stress is much larger than the viscous stress. As already mentioned, this condition is *not* satisfied everywhere in the boundary layer. Figure 4 shows the Reynolds shear stress distribution at four different Reynolds numbers. (Some details of how these distributions were obtained are given in the figure caption, and more can be found in section 2.3.) Also shown in figure 4 is the viscous shear stress distribution. For reasons that will soon become clear, the distance from the wall is normalized by the so-called wall variables, which are the kinematic viscosity coefficient ν of the fluid and the friction velocity $U^* = \tau_w^{1/2}$, τ_w ($= \nu \partial U/\partial y$ at the wall) being the kinematic wall shear stress.

One can identify several fairly distinct regions in figure 4. Very near the wall, there is a small region in which the viscous stress is overwhelmingly large compared to the turbulent shear stress. For a certain distance beyond this region, neither the viscous stress nor the turbulent shear stress is negligible. This region merges with another within which τ is nearly a constant and equal to τ_w at high Reynolds numbers. (We shall return to the low Reynolds number cases later.) Even further away from the wall, τ drops off to zero gradually. These various regions are described in greater detail below.

2.1. The viscous layer: The region closest to the wall in which the viscous shear stress is dominant is called the *viscous sublayer*. To a first approximation, it is reasonable to think that the entire shear stress in this layer is the result of viscous action, which implies that the only quantities of relevance are U^* and ν. It follows from the definition of the shear stress that the velocity variation in the sublayer is linear with the distance from the wall, and is given by

$$U/U^* = yU^*/\nu. \qquad (1)$$

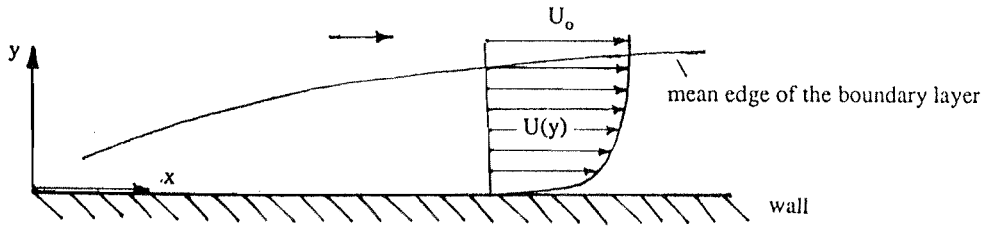

Figure 3. The schematic of the boundary layer defining coordinates.

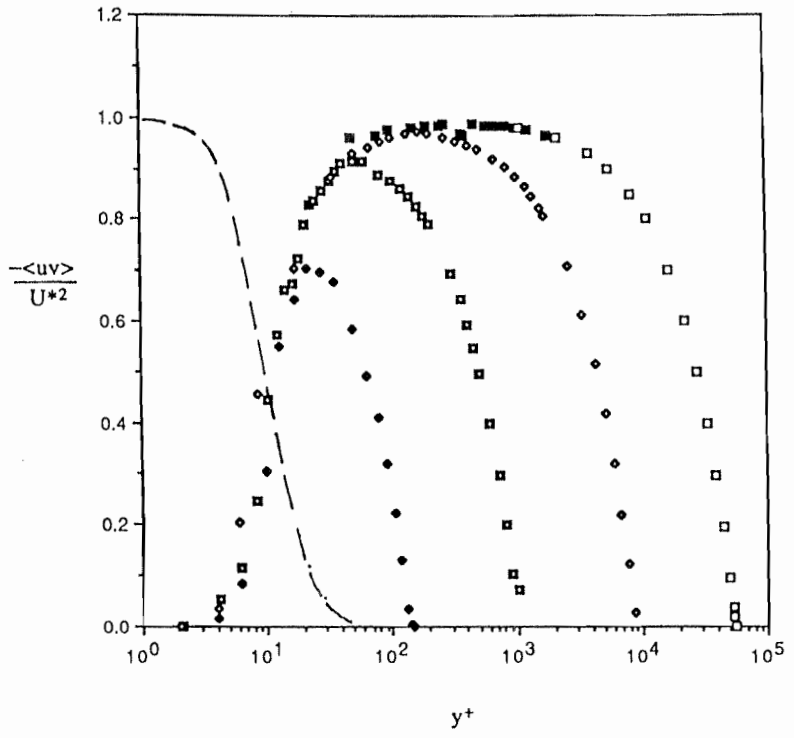

Figure 4. The viscous and turbulent shear stresses in pipe flows. The region up to and including the constant-stress layer is similar to that in the boundary layer. We chose pipe data because the shear stress can be computed from mean velocity using equation (18), section 2.3. The dashed line is the viscous stress. From left to right, the calculated Reynolds stresses correspond to: Nikuradse (1932), $R^* = U^*a/\nu = 140$; Laufer (1954), $R^* = 1050$: Laufer, $R^* = 8600$; Nikuradse, $R^* = 5.54x104$; a is the pipe radius. For the last flow, the closest velocity measurement is at y^+ of 1110, and points plotted at smaller y^+ are based on a reasonable extrapolation of the measured mean velocity. They may therefore be somewhat uncertain.

It is convenient to introduce the superscript + which refers to the normalization by wall variables. In this notation, equation (1) becomes $U^+ = y^+$. It is known from empirical data that the height of the viscous sublayer is on the order of $5\nu/U^*$, where the combination ν/U^* is called the wall or viscous unit of length.

As already noted, the viscous action extends substantially beyond the viscous sublayer. If we define, for definiteness, this layer to be one in which 95% of the direct viscous dissipation occurs, its thickness, to within experimental uncertainties, is on the order of 30 wall units. (This number may vary somewhat with the various flow conditions, but it is not much.) We shall designate this layer as the *viscous layer*. The thickness of the viscous layer as a function of the momentum thickness Reynolds number (R_θ) is shown in figure 5. Although it occupies about 25% of the total thickness at the lowest Reynolds number that turbulent boundary layers are known to exist (R_θ of about 350, see Preston 1958), it is a small fraction of the total boundary layer thickness at high Reynolds numbers. But its importance far exceeds its size, with more than a third of the turbulent energy being produced here. (This last statement is the result of integrating the distributions of turbulent energy production at several Reynolds numbers up to the highest value for which reliable measurements are available. Whether this is in principle true in the limit of infinitely large Reynolds number cannot be decided simply; we indicate in section 2.4 a crucial point that needs to be settled for a satisfactory resolution of the problem.)

The region of the viscous layer outside of the viscous sublayer is often called the *buffer layer* ($5 \leq y^+ \leq 30$, approximately). The peak production and dissipation of turbulent energy, already mentioned in section 1, occur in the middle of the buffer layer where the viscous and turbulent stresses are approximately equal. To within experimental uncertainty, this height corresponds to y^+ of about 12 (see figure 4). A close examination of the available data indicates that this result is independent of Reynolds number; again, the asymptotic validity of this statement is related to the issue raised in the preceding paragraph.

In the close vicinity of the wall, all flow quantities can be expanded by the Taylor's series, equation (1) for the mean velocity being only the first term in such an expansion. From considerations of the no-slip condition, and continuity and dynamical equations, Monin & Yaglom (1971) show that the appropriate expressions for the mean and fluctuating velocity are of the form

$$U^+ = y^+ - a y^{+4} + b y^{+5} + \ldots \tag{2a}$$

$$u'^+ = a_1 y^+ + b_1 y^{+2} + \ldots \tag{2b}$$

$$v'^+ = a_2 y^{+2} + b_2 y^{+3} + \ldots \tag{2c}$$

$$w'^+ = a_3 y^+ + b_3 y^{+2} + \ldots \tag{2d}$$

$$-\langle uv \rangle^+ = a_4 y^{+3} + b_4 y^{+4} + \ldots \tag{2e}$$

Primes here and elsewhere denote root-mean-square *(rms)* values. Note the absence of the second and third order terms in the expansion for the mean velocity, and of the first order term in (2c) for normal velocity fluctuations; also, the leading term in the Reynolds shear stress expansion is of order y^{+3}. Since in the viscous layer the sum of the viscous stress and the Reynolds shear stress is a constant – this being readily apparent, to the lowest order, from the equations of motion – it

follows that $a_4 = 4a$, and $b_4 = -5b$. There is no first-principles theory that gives these coefficients, and it is difficult to determine them *accurately* from experimental data. Both the constants in the mean velocity can be determined more reliably than those for fluctuations (although their *absolute* accuracy is not very high), and a reasonable fit to data from several experiments turn out to be $a = 10^{-4}$, $b = 1.6\times10^{-6}$. Equation (2a) with these numerical values for the coefficients is valid for $y^+ < 20$. Rough estimates for other leading coefficients provided by Monin & Yaglom are $a_1 = 0.3$, $a_2 = 0.008$ and $a_3 = 0.07$.

Figure 6 shows the *rms* intensities of the three fluctuation velocity components normalized by U^*. Careful measurements by Kreplin & Eckelmann (1979) near the wall show (figure 7) that the streamwise and spanwise fluctuations normalized by the local mean velocity have finite non-zero limiting values, whereas that in the direction y possesses a zero limit. While the fluctuations vanish at the wall, figure 7 also shows that they rise to rather high relative levels fairly quickly in the viscous layer. Although relatively large, the sublayer fluctuations are not capable of transmitting momentum (figure 4). Further, they are not responsible for significant production or dissipation of turbulence (although they are marginally more effective at dissipation than at production). A conceivable conclusion is that the viscous sublayer performs little dynamic function, merely providing the right boundary condition to the rest of the flow. A strong evidence for this comes from comparisons between rough-wall and smooth-wall boundary layers. As long as the roughness elements are confined to the viscous sublayer, their effect on the mean velocity distribution outside of the sublayer is negligible.

Expressions (2) enable us to deduce the *rms* fluctuating vorticity components at the wall. Since the derivatives of averages with respect to x and z vanish at the wall, it follows that

$$\omega'_x(y=0) = 0.07U^{*2}/\nu,\ \omega'_y(y=0) = 0,\ \text{and}\ \omega'_z(y=0) = 0.3U^{*2}/\nu. \qquad (3)$$

Here, ω_x, ω_y and ω_z are the fluctuating vorticity components in x, y and z directions respectively. Thus, even though the wall (except at the leading edge) is *not* a source of mean vorticity, there is a concentration of fluctuating vorticity there. The vorticity components at the wall can also be estimated from the knowledge of the limiting behavior of velocity fluctuation intensities shown in figure 7 or the fluctuating shear stress measurements right at the wall (e.g., Fortuna & Hanratty 1971, Sreenivasan & Antonia 1977). The conclusions that follow are:

$$\omega'_x(y=0) = 0.065U^{*2}/\nu,\ \omega'_y(y=0) = 0,\ \text{and}\ \omega'_z(y=0) = 0.24U^{*2}/\nu. \qquad (4)$$

The direct numerical simulations of Moin & Kim (1982) show (figure 8) that

$$\omega'_y\,(y=0) = 0,\ \omega'_z\,(y=0)/\omega'_x\,(y=0) = 1.5. \qquad (5)$$

The ratio is much smaller in experiments, and it is not clear whether this is merely a consequence of difficulty in numerically resolving the viscous sublayer. Note that the numerical simulations show that the largest ω_x and ω_z components occur at the wall, and are diffused outwards. The largest ω_y component is produced somwhere in the middle of the viscous layer, and is diffused both inwards and outwards.

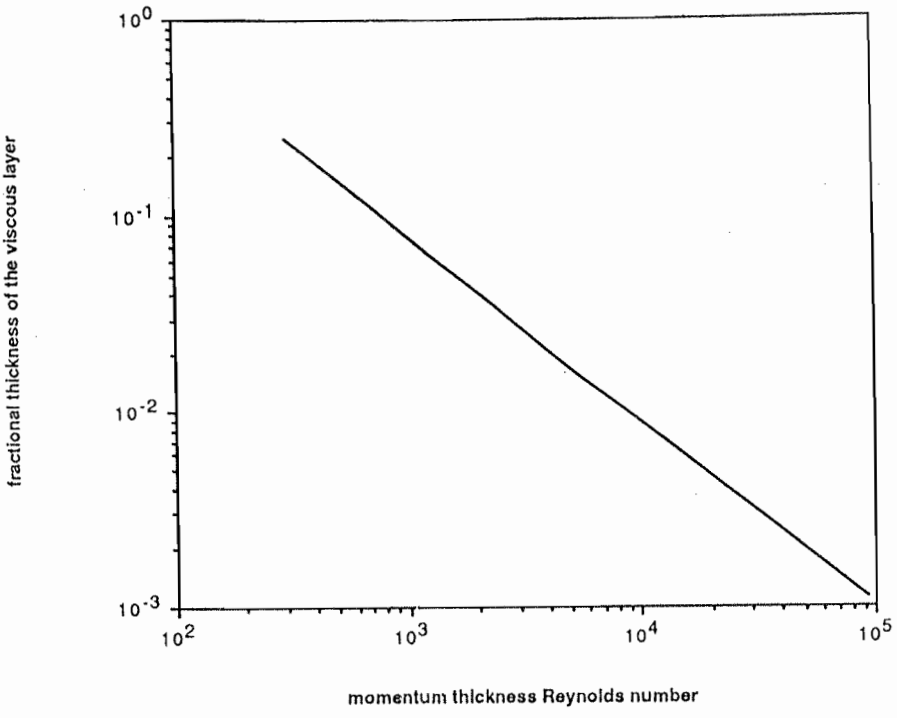

Figure 5. The thickness of the viscous layer as a fraction of the boundary layer thickness.

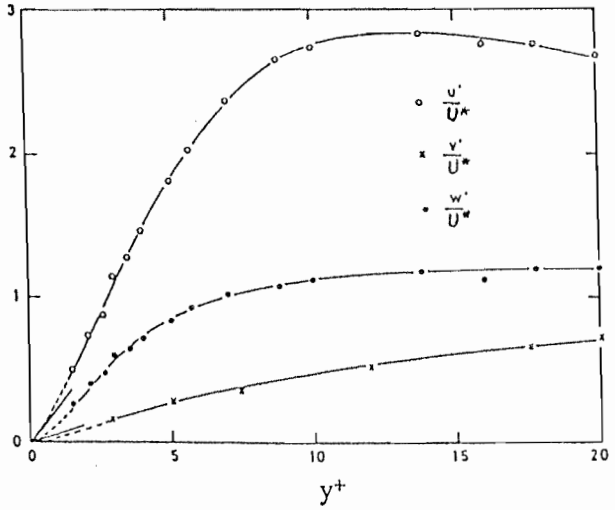

Figure 6. The distribution of u', v', and w' normalized by the friction velocity U^*. Data from Kreplin & Eckelmann (1979).

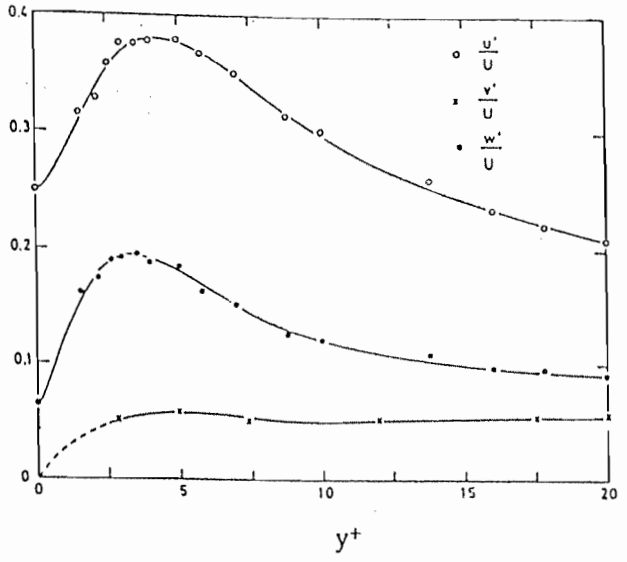

Figure 7. The distribution of u', v', and w' normalized by the local mean velocity U(y). Data from Kreplin & Eckelmann (1979).

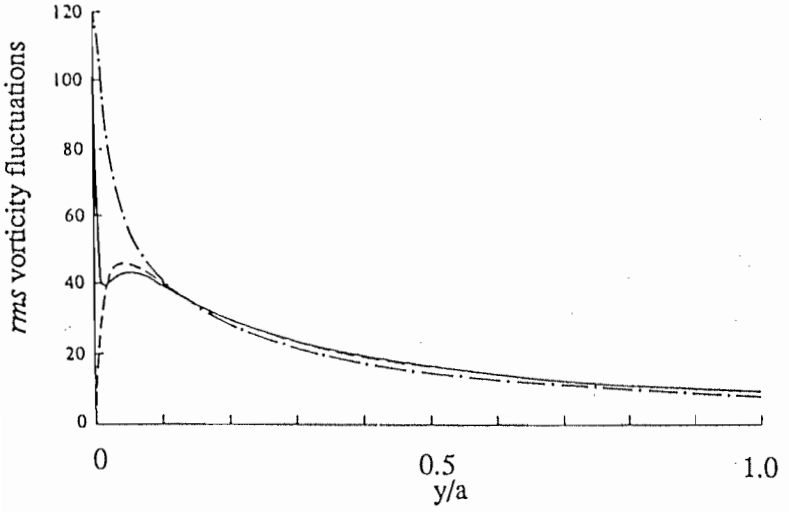

Figure 8. The *rms* vorticity fluctuations resolved in the direct numerical simulations of Moin & Kim (1982). ——, ω'_x, – – –, ω'_y, – . – , ω'_z.

2.2.The constant-stress layer: Outside the viscous region, the turbulent shear stress is many times greater than the viscous stress, which is the same as saying that the momentum flux across layers of fluid is accomplished nearly entirely by turbulence. We see from figure 4 that this region is substantial at high Reynolds numbers, and characterized by an approximately constant Reynolds shear stress. Hence, the variation of the mean velocity in this region must not depend on fluid viscosity but only on the turbulent stress transmitted across it. We are discussing here the variation of the velocity, not its absolute value, this being so because the addition of an arbitrary constant velocity will not change the momentum flux. The precise value of the velocity in the constant-stress region will depend on the 'boundary condition' provided by the viscous layer. Dimensional analysis gives

$$\partial U/\partial y = (1/\kappa)\tau^{1/2}/y, \tag{6}$$

where the constant κ is named after von Kármán, and is presumed to be 'universal' (see section 2.4). In writing (6) we explicitly assume that the only relevant length scale in this region is the distance from the wall y; neither the viscous length ν/U^* nor the boundary layer thickness δ is relevant, the former because it is very small compared to y and the latter because y/δ is very small. The validity of (6) depends on these two conditions, which can empirically be ascertained to hold at large Reynolds numbers.

It can be seen from figure 4 that the Reynolds shear stress in this region is equal to the wall stress τ_w, so that (6) can be written as

$$\partial U/\partial y = (1/\kappa)U^*/y.$$

Integrating, we have

$$U(y) = (1/\kappa)U^*\log(y) + A. \tag{7}$$

Consistent with previous remarks, the constant A should depend on boundary conditions arising from the existence of the viscous layer underneath. If we assume that the velocity at the edge of the viscous layer, defined by $\beta\nu/U^*$, can be expressed as αU^*, where α and β are dimensionless constants, we get

$$A = \alpha U^* - (1/\kappa)U^*\log(\beta\nu/U^*) = (1/\kappa)U^*\log(U^*/\nu) + BU^*. \tag{8}$$

We can then write (7) as

$$U^+ = (1/\kappa)\log(y^+) + B \tag{9}$$

for all $y >> \nu/U^*$; for the smooth-wall case case considered here, B is expected to be another 'universal' constant. The constants κ and B have so far not been determined from first principles. Typical empirical values are $\kappa = 0.41$ and $B = 5.5$.

The mean velocity distribution given by (9) is the so-called log-law. It can be derived by other arguments also, Millikan's (1939) asymptotic arguments among them, but they all depend on the existence of the constant stress layer. (For a different view, see section 2.4.) The log-law (see figure 9) does not extend all the way to the viscous sublayer but smoothly blends with equation (2a).

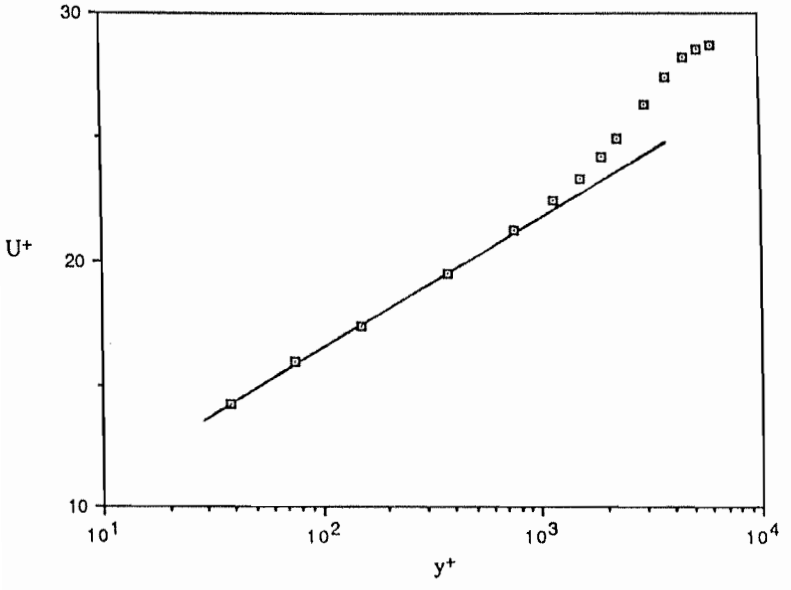

Figure 9. A typical semi-logarithmic plot, from the flat plate data of Weighardt & Tillmann (1951). Free stream speed U_0 = 33 ms^{-1}, the momentum thickness Reynolds number R_θ = 15160, the shape factor H = 1.31. Deviations from log-law are generally perceptible below a y^+ of 30 (viscous region); the measurements given here do not extend to the viscous region.

The requirement that the turbulent stress be constant for the logarithmic region to exist is not stringent because only the half power of the turbulent stress appears in the above equations. The constant-stress region can therefore be interpreted generously to include the entire region 'within the −3dB points' of the peak stress (that is, the region within which the stress value is 70.7% of the peak) without losing accuracy. Examination of all the available experimental data suggests the following bounds for the constant stress region:

$$\text{lower bound: } y^+ = 30 \tag{10a}$$

$$\text{upper bound: } y^+ = 0.2R^*. \tag{10b}$$

Here, $R^* = U^*\delta/\nu$, δ being the boundary layer thickness. It is convenient to think of the Reynolds number R^* as the ratio of the boundary layer thickness (the outer scale) to the viscous length scale ν/U^*.

Since it is the half-power of the stress (namely U^*) that is the relevant quantity, the log-law (with the same value of the constant κ) has been observed under a variety of circumstances where it is not expected to be valid *a priori*. One such example is the low Reynolds number wall flow where the constant-stress region is essentially non-existent, and the maximum Reynolds shear stress is substantially less than the wall stress (see figure 4); another is the case of mild pressure gradients whose influence on the stress distribution itself is significant but negligible on the mean velocity.

Velocity variations in viscous sublayer and constant-stress region depend only on y^+, and it is therefore useful to include the buffer layer into this description – even though neither (1) nor (9) is valid there – and write the velocity distribution in the so-called inner layer encompassing the entire region from the wall to the outer edge of the 'constant-stress' region as

$$U^+ = f_i(y^+). \tag{11}$$

This is the so-called inner law of velocity distribution, first formulated by Prandtl (1925).

The flow close to the wall (including the logarithmic part) is essentially the same in boundary layers, pipes and channel flows, and altogether encompasses about a fifth of the boundary layer thickness, pipe radius or channel half-height. (With slightly readjusted constants κ and B, it holds almost up to the centreline in pipes and channels.) This is a strong indication that the important dynamics of that region are controlled essentially by the total stress transmitted, and not by other details.

2.3. Fluctuating quantities in the constant-stress region: This last fact imposes some dynamic constraints on the flow. In a broad sense, these have been set forth by Townsend (1976), and enlarged by Perry & Abell (1975); see also Tennekes & Lumley (1972, Chapter 5) and section 2.6. Dimensional arguments similar to those above show that fluctuation intensities in the constant stress layer must be constant also (to the lowest order, to the same degree of approximation as the shear stress). This has been verified experimentally (see figure 10 for u'), and some typical values are

$$u'/U^* = 2.0,\ v'/U^* = 1 \text{ and } w'/U^* = 1.4. \tag{12}$$

It also follows that the average energy dissipation rate $\langle\varepsilon\rangle$ and production rate $\langle p\rangle$ must vary inversely with distance from the wall so that we can write

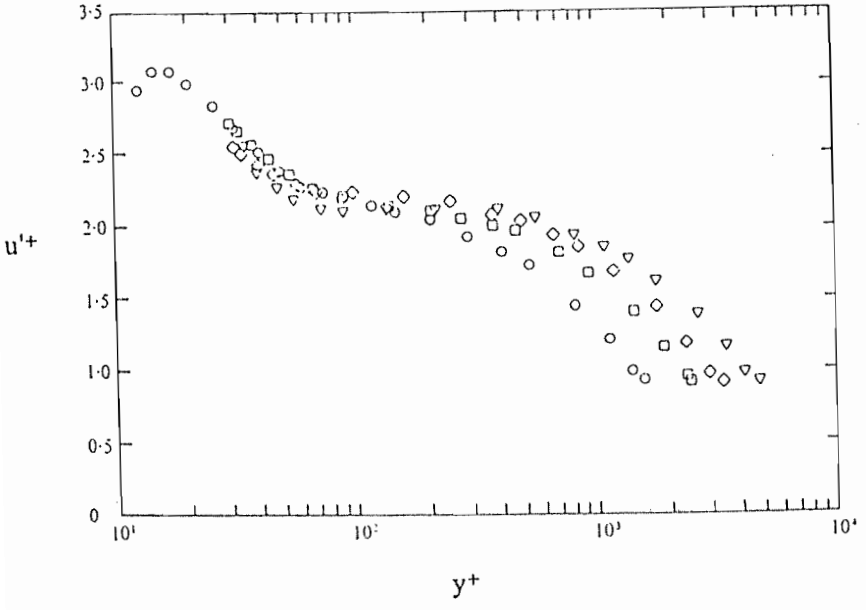

Figure 10. Streamwise turbulence intensity in the wall region of a pipe flow, from Perry & Abell (1975). O, Re = 7.8×10^4; □ 13.3×10^4; ◊, 17.3×10^4; ∇, 25.7×10^4.

$$\langle\varepsilon\rangle = \langle p\rangle = U^{*3}/\kappa y. \tag{13}$$

Figure 11, in which the ordinate is $(\langle p\rangle\delta/U^{*3})\kappa$ and the abscissa is y/δ, shows an extensive straight line region of slope −1, confirming (13) adequately. (There is no special significance to the use of δ as the normalizing length because it appears in both the abscissa and the ordinate.) Similarly, one can write the *rms* vorticity fluctuation in the direction i as

$$\omega_i'\nu/U^{*2} = C_i/y^+. \tag{14}$$

Vorticity fluctuations from computations confirm this conclusion (figure 12). Measurements are rather sparse and it is uncertain that they support (14); also, the constant C is different in the two sets of measurements shown in figure 12. Clearly, more work is needed.

One can also obtain specific results for the spectral form in the constant-stress region. From the knowledge that there is in this region no preferred length scale other than the distance from the wall, and that the dynamics there is governed by the turbulent shear stress transmitted across different fluid layers, one can write the energy spectral density $\phi(ky)$ in the form

$$\phi(k) = DU^{*2}y\ \zeta(ky). \tag{14}$$

Here, k is the wave number magnitude, $\int\phi(k)\,d(k) = \langle u^2\rangle$, and $\zeta(ky)$ and D are expected to be a universal function and a universal constant respectively. Similar expressions hold for the other two components. If we argue that the spectral density should not depend on y (because not much distinguishes one layer from another in the constant stress region; see below), $\zeta(ky)$ has to be of the form $(ky)^{-1}$, and we are left with the result

$$\phi(ky)/U^{*2} = D/ky. \tag{15}$$

Figures 13 and 14 show that this is valid over an extended wave number regime $ky < 1$. It is therefore clear that small changes in y will not affect its dynamics; this is the *a posteriori* justification for expecting the spectral density in that region to be independent of y. From the experimental data, one can estimate D to be of the order unity. Note that figure 14 is for fluctuations in wind speed over sea, and is measured 200 m above the mean water level in the sea; we therefore emphasize that, even when the flow underneath the log-region is vastly different in the two cases, the same relation is valid at the low wave number end of the spectrum (which, for convenience, will be denoted the energy containing range).

Obviously, (15) is valid only for the stress- (or energy-) carrying scales, and is not expected to hold either on the low end which depends on eddies characteristic of the flow width, or on the high end where viscous effects are important. This latter fact can be seen explicitly in figures 13 and 14: At large enough wave numbers, we have the usual −5/3 law of Kolmogorov; even at moderate Reynolds numbers, the −5/3 region extends all the way to the high end of (15). The first feature is not evident in figures 13 and 14 because the data do not extend to low enough wave numbers. But it can be seen clearly in figure 15 taken from Perry & Abell (1975).

Closer to the wall where viscous effects are also important, we expect to have:

$$u'/U^* = f_1(y^+)$$

$$v'/U^* = f_2(y^+)$$

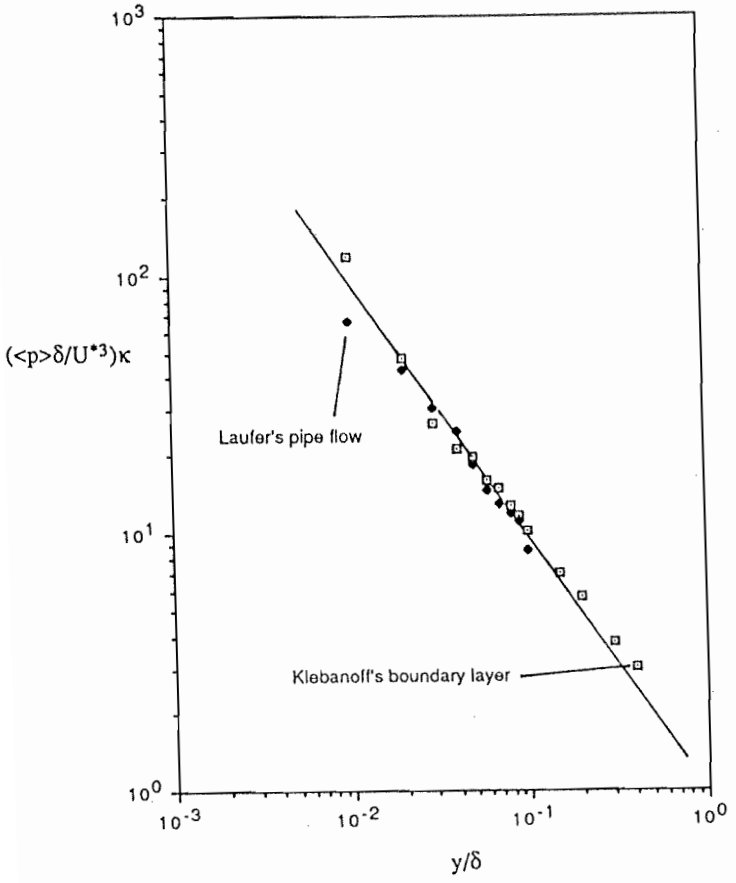

Figure 11. Non-dimensional turbulent kinetic energy production in the constant-stress region. Data from Laufer's (1954) pipe flow and Klebanoff's (1955) boundary layer.

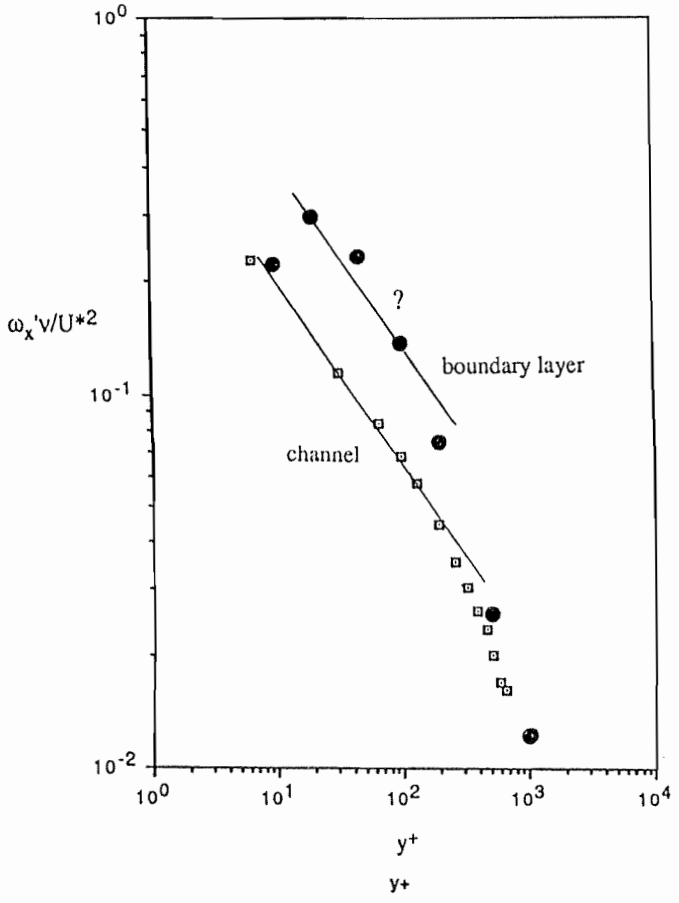

Figure 12. Non-dimensional vorticity fluctuation data from measurement (Wallace 1986, boundary layer), and direct numerical simulations (Moin & Kim 1982, channel).

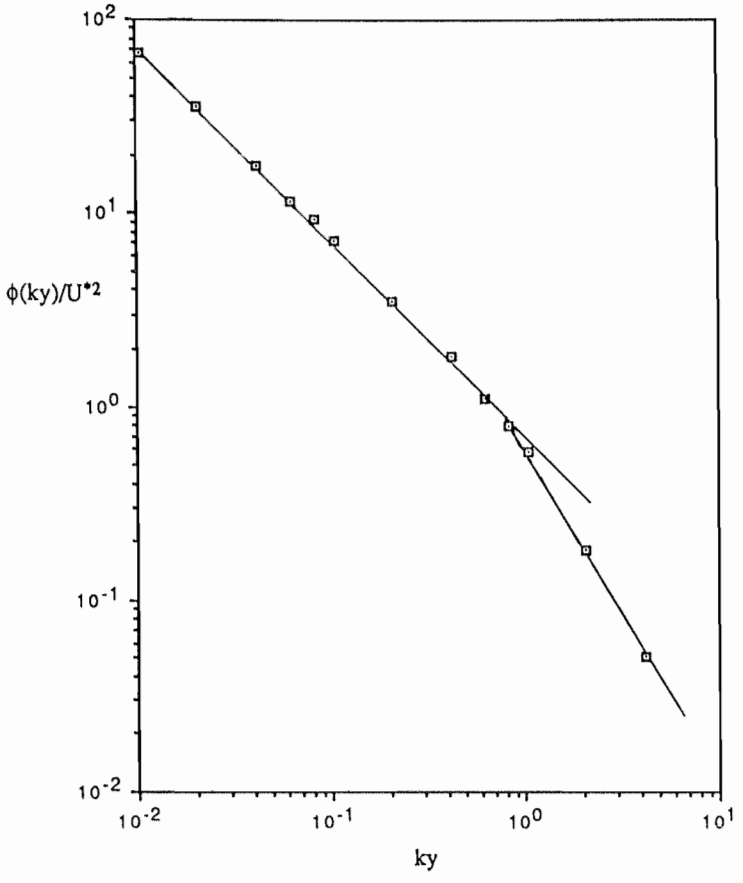

Figure 13. The −1 power law displayed in the pipe data of Laufer (1954), The power law at higher wave numbers is the Kolmogorov's −5/3 law. There is no discernible range of intermediate scales for which neither is valid.

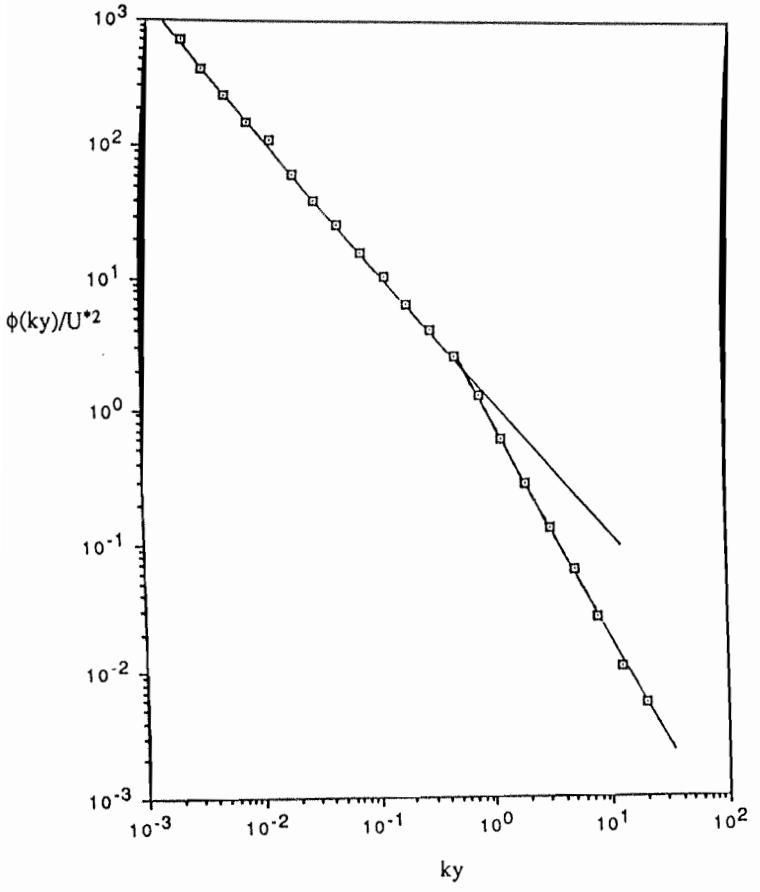

Figure 14. The wind data over the ocean (Pond et al. 1966) displaying the −1 and −5/3 power laws.

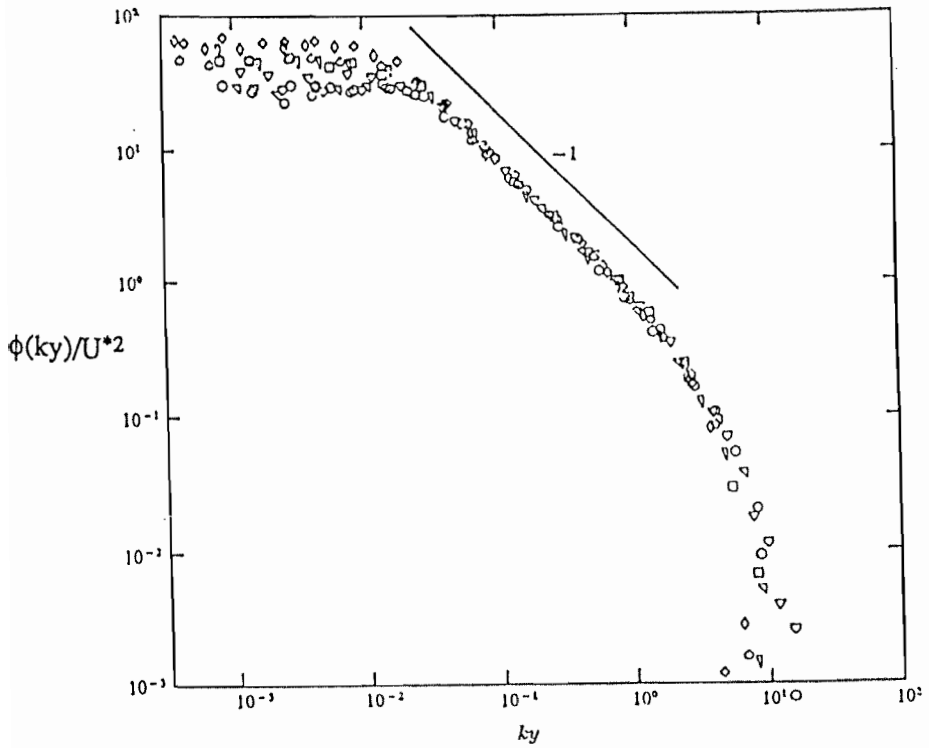

Figure 15. Pipe data of Perry & Abell (1975) show that there are very large scale fluctuations outside of the equilibrium hypothesis; these constitute the so-called inactive motion. The small scale features lying outside the equilibrium range may either obey the usual −5/3 law (figures 13 and 14) if the Reynolds number is sufficiently high, or simply be viscosity-dependent, at low Reynolds numbers.

	$Re \times 10^{-3}$	y^+	y/R	U/u_τ
○	80	150	0·0934	17·6
□	120	100	0·043	16.6
▽	120	150	0·0645	17.59
▽	120	200	0·086	18·3
◇	180	104	0·03	16·6
◁	180	138	0·04	17·31
◇	180	275	0·08	19·2
✣	260	148	0·03	17·6
◇	260	246	0·05	18·8
◁	260	444	0·09	20·4

$$w'/U^* = f_3(y^+)$$

$$(<p>/U^{*3})\kappa y = f_4(y^+)$$

$$(<\varepsilon>/U^{*3})\kappa y = f_5(y^+)$$

$$\phi(k^+) = \phi(k^+, y^+).$$

Not enough work has gone into determining these empirical functions.

The arguments used in deriving the spectral form (15) are qualitatively similar to those employed by Kolmogorov (1941) in discussing the energy cascade. We recall that in this theory the spectral shape in the inertial subrange is completely detemined at high Reynolds numbers by the energy flux across the wave number domain. The analogy here is the following: The primary boundary condition on the boundary layer dynamics is that the wall provides a sink of momentum, similar to the energy sink at fine scales in the Kolmogorov scenario. This loss has to be replenished constantly by the outer stream *via* the momentum flux across different 'fluid layers' in the turbulent boundary layer, qualitatively analogous to the energy flux across the wave number domain. Just as in Kolmogorov's spectral theory, it is plausible to expect this process of momentum flux in physical space to determine, to a first approximation, the average dynamics in the constant-stress region.

Another point can be brought to bear by examining the locations in the boundary layer where the largest *rms* fluctuations occur. In figure 16 is plotted the distance from the wall where the streamwise fluctuation peaks. It appears that this height in wall variables is sensibly independent of the Reynolds number. Similar data (figure 17) on the normal component show larger scatter, perhaps reflecting the difficulty in measuring it accurately in the wall region and the fact that the peak in the v' distribution is rather flat; in spite of the scatter, it is clear that the location of this peak is a strong function of the Reynolds number. A rough fit to the data is given by the relation

$$y^+_{v'max} = R^{*0.75}, \tag{16}$$

suggesting that v-fluctuations are essentially an outer layer (and therefore inviscid) phenomenon. Similar data on the spanwise component are rather sparse (figure 18). Even though the position of peak v' does not scale on wall variables, and the conclusion on w' is uncertain, the total fluctuation energy does so because, near the wall, it is essentially overwhelmed by the streamwise component.

The peak Reynolds shear stress occurs at increasingly higher y^+ at increasing Reynolds numbers (figure 19a); as a fraction of the boundary layer thickness, however, the peak location moves closer to the wall. A simple equation fitting the data is

$$y_p^+ = 2R^{*0.5}. \tag{17}$$

Since accurate measurement of the Reynolds shear stress near the wall is beset with several problems including the probe size, it would be valuable to corroborate (17) by some other means. As already noted, the wall layer dynamics in the boundary layer is the same as that in pipe and channel flows; for the latter two in the fully developed state, the Reynolds stress distribution is related exactly to the mean velocity distribution U(y) by

$$-uv = -\nu(du/dy) + U^{*2}(1-y/a), \tag{18}$$

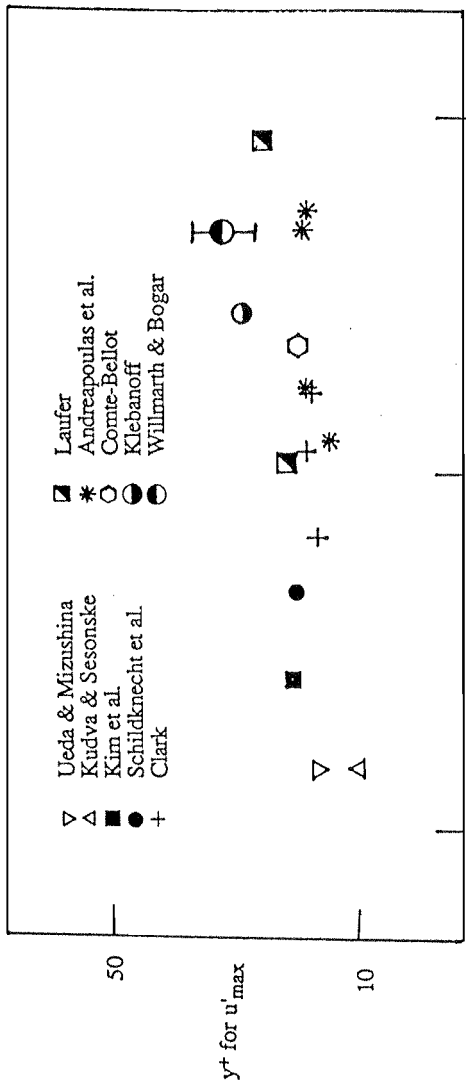

Figure 16. The location of the peak in u', plotted in wall units, as a function of the Reynolds number R^*.

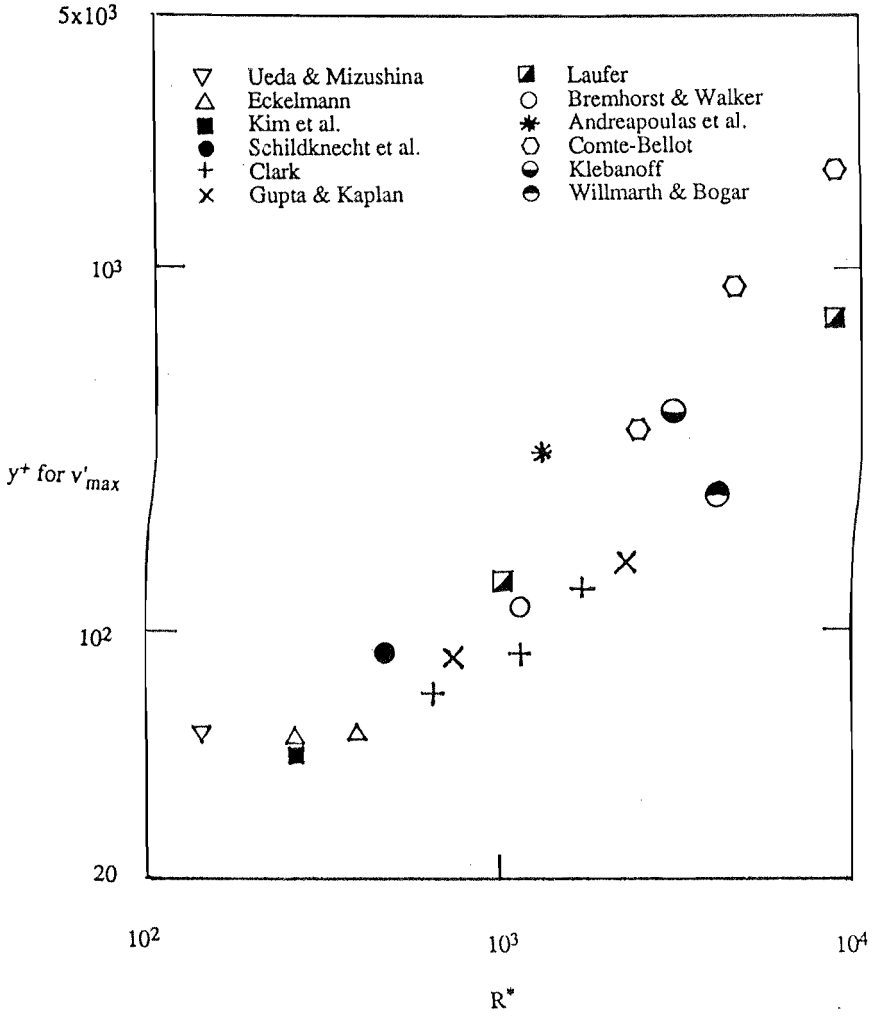

Figure 17. The location of the peak in v', plotted in wall units, as a function of the Reynolds number R^*.

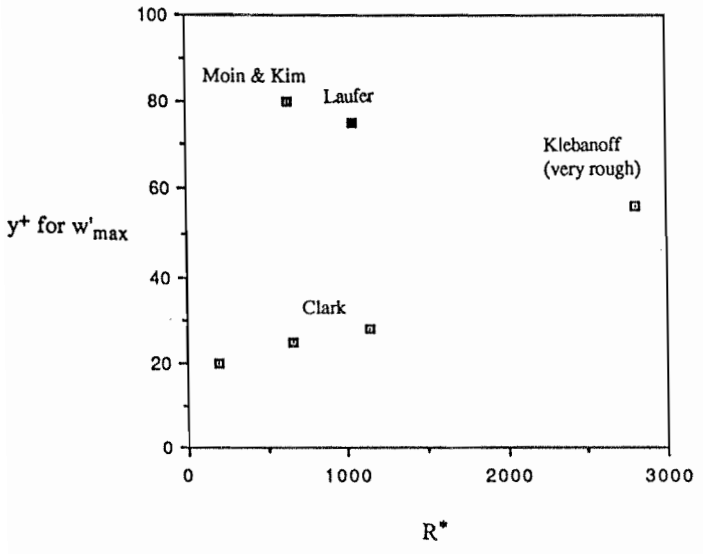

Figure 18. The location of the peak in w', plotted in wall units, as a function of the Reynolds number R^*.

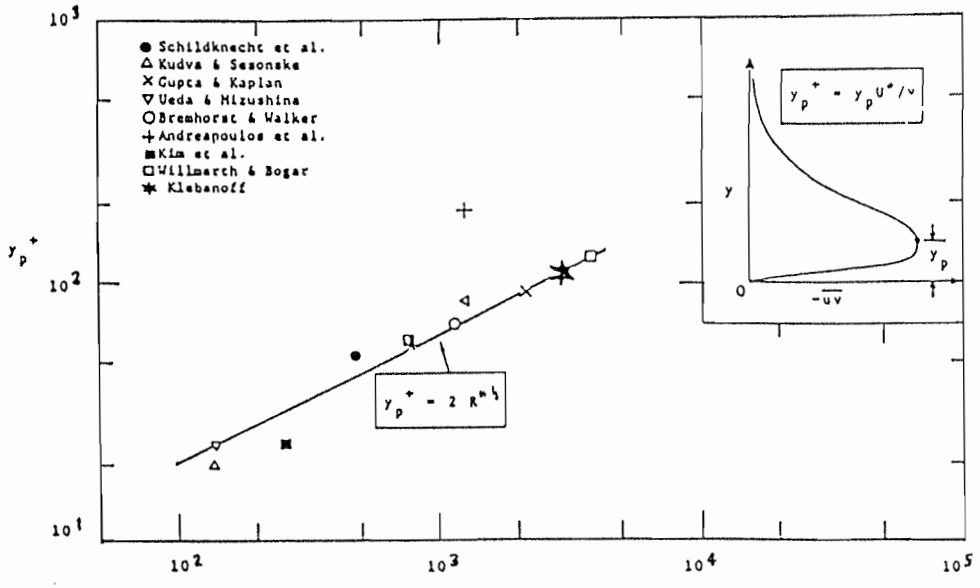

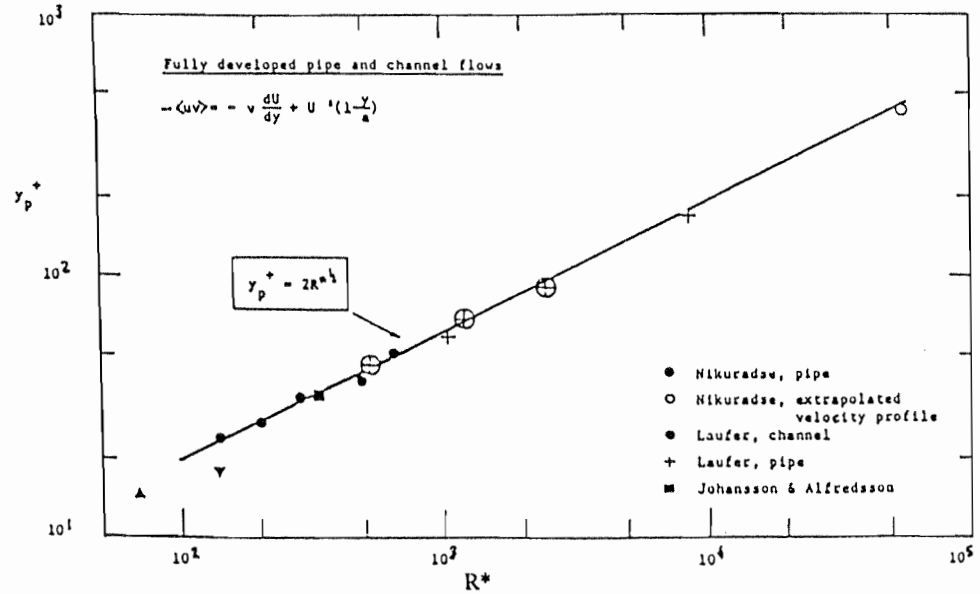

Figure 19. The peak Reynolds shear stress location in boundary layer, pipe and channel flows. (a) Data from various experiments. (b) Data computed from measured mean velocity distributions at various Reynolds numbers. See equation (18).

where a is the channel half-height or pipe radius. Mean velocity measurements are generally accurate, and so the computed shear stress distribution can be expected to be quite reliable. The results obtained in several flows (figure 19b) substantiate (17) satisfactorily. (For a more detailed commentary on the experimental data, see Sreenivasan 1987.) It is clear that at high Reynolds numbers the peak stress occurs substantially outside the viscous region.

The fact that the peak Reynolds shear stress follows (17) in the turbulent boundary layer as well as pipe and channel flows is interpreted to mean that, in all these flows, the motion producing the Reynolds shear stress does not primarily reside at constant y^+. Taken together with the earlier remark that the position of the maximum kinetic energy scales on wall variables, this leads to the conclusion that the energy and stress carrying eddies are quite different. It was primarily to obviate the need for this awkward conclusion that Townsend (1961) and Bradshaw (1967) invoked the so-called inactive motion, the part of the energy containing motion that does not scale on the Reynolds shear stress.

2.4. The power-law variation of the mean velocity distribution: We have tried to describe the boundary layer structure in terms of self-similarity arguments that make the underlying assumptions rather transparent, but a little closer examination is helpful. In general, the state of the motion at some point in the inner layer can be expected to depend on the turbulent shear stress τ, the viscosity coefficient ν, the distance from the wall y, and the boundary layer thickness δ. Thus

$$\partial U/\partial y = f(\tau,\nu,y,\delta). \tag{19}$$

We can write this non-dimensionally as

$$y(\partial U/\partial y)/U^* = g(y^+, R^*). \tag{20}$$

If the function g asymptotes to a constant in the limit of $y^+ \to \infty$ (which clearly implies $R^* \to \infty$), we can write

$$y(\partial U/\partial y)/U^* = \text{constant}$$

and recover the log-law discussed earlier.

In general, there is no special reason to anticipate that the limiting form of the function g is well-behaved. It could, for instance, diverge in some power-law fashion on the parameter y^+. We can then write (20) alternatively as

$$y(\partial U/\partial y)/U^* = (y^+)^\lambda\, h(R^*),$$

where λ is a parameter that might depend on R^*. Barenblatt (1979) has called this the incomplete self-similarity in the parameter y^+, and has explored its consequences. Following him, we integrate the above equation and write

$$U^+ = (y^+)^\lambda/(\lambda\kappa(R^*)) \tag{21}$$

where $\kappa(R^*)$ is $1/h(R^*)$. This shows that the variation of the mean velocity occurs according to a power law. Power laws, although in use in the turbulence literature for a long time, have come to be discredited since Millikan (1939) derived the log-law from asymptotic arguments. However, the basis for them is *a priori* as sound as for the log-law, especially at low Reynolds numbers.

Barenblatt has also presented a preliminary anlaysis of the experimental data in pipe flows of Nikuradse (1932), and shown that κ is essentially independent of R^*; while, on the other hand, λ does vary as shown in figure 20. Although it is hardly possible to distinguish power-laws with such small exponents from logarithmic variation, and the differences are immaterial from an experimental point of view, it makes a fundamental difference to our understanding of the boundary layer asymptotics. Of particular interest is the limiting behavior of the constant λ as $R^* \to \infty$. If λ goes to zero, we recover the log-law as before. On the other hand, if the limiting value is a non-zero constant, the log-law does not strictly hold, and the dependence on viscosity of the velocity distribution in the boundary layer will be nontrivial even at infinitely large Reynolds numbers.

The log-law scenario has been questioned in the past by Long & Chen (1981). A moment's reflection with respect to figure 4 shows that the constant-stress region (and therefore the log-law) does not obtain if the lower limit for the effective constant-stress region, namely equation (10a), is replaced by $R^{*\alpha}$, where α is any small positive number. Unfortunately, it is not possible from experiments either to dismiss such a possibility or support it. The chief difficulty is the paucity very near the wall of experimental data on the Reynolds stress at truly high Reynolds numbers. One might think that in pipe and channel flows the turbulent shear stress can be inferred from the mean velocity data using (18), but sufficiently accurate mean velocity data is also not available close enough to the wall at truly high Reynolds numbers. This important problem is therefore unresolved at present, but it is this that bears strongly on whether the earlier statements in section 2.1 about turbulence production in the viscous region are valid asymptotically.

2.5. The outer layer: The mean velocity profile in the outer part of the boundary layer is characterized by the velocity defect $U_o - U(y)$, where U_o is the free-stream velocity. The previous assertion (section 2.3) that the momentum flux is the primary governing factor suggests that the wall is felt entirely through the friction velocity U^*, from which it follows that the only quantities on which the defect velocity can depend are U^*, U_o, y, and δ. We can then write

$$(U_o - U(y))/U^* = \text{fn}(y/\delta, U^*/U_o). \tag{22}$$

Experiments show that the dependence of the defect velocity ratio on U^*/U_o is rather weak (if at all) so that one can write

$$(U_o - U(y))/U^* = f_o(y/\delta). \tag{23}$$

This so-called defect law, first formulated by von Kármán (1930), is well confirmed by experiment (figure 21). The defect law applies even to the logarithmic region.

Coles (1956) has combined the defect law and the inner law by writing the velocity distribution at any height as

$$U(y)/U^* = f_i(y^+) + (\Pi/\kappa)\, w(y/\delta), \tag{23}$$

where Π is a constant, and $w(y/\delta)$ is the so-called wake function. The constant Π depends strongly on the Reynolds number for small Reynolds numbers, and may asymptote (Coles 1962) or vary only little (Crocco 1965) for $R_\theta > 6000$. The emphasis in this formulation is that, in the outer layer,

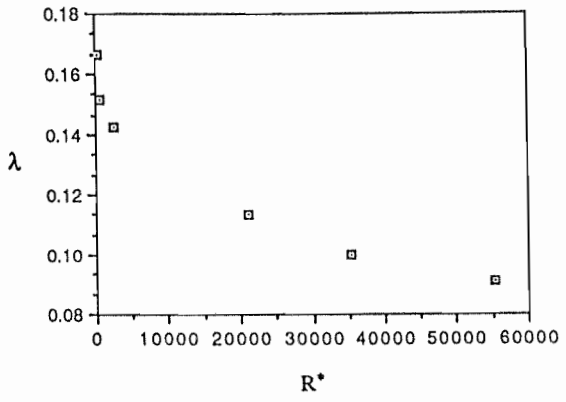

Figure 20. The Reynolds number variation of the power-law exponent from Nikuradse's pipe flows. Nikuradse's own power-law exponent is 0.1 for the highest two Reynolds numbers, but our fit to his data shows that, while a range of exponents is possible, the best value for the highest Reynolds number is somewhat different as shown; other values are Nikuradse's.

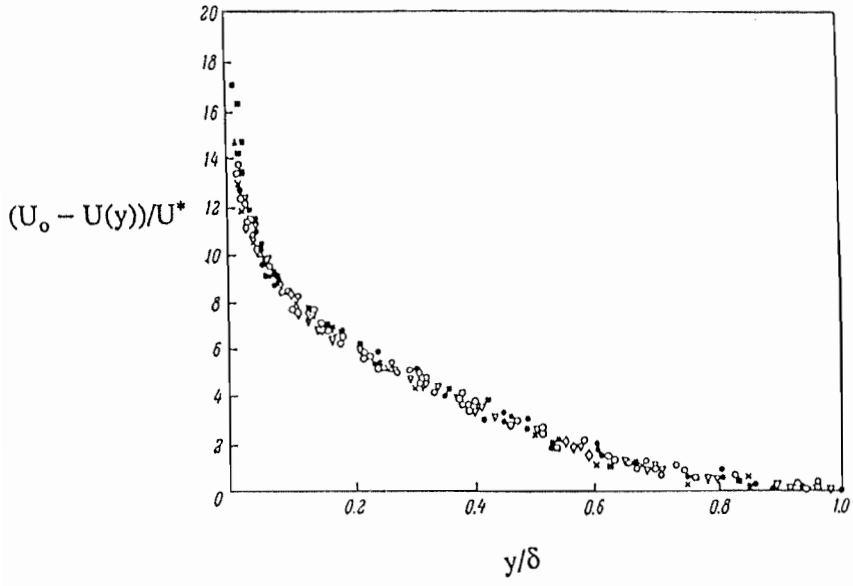

Figure 21. Verification of the defect law for the turbulent boundary layer, according to data from different authors (different symbols). Figure taken from Monin & Yaglom (1971).

the departure of the measured velocity distribution from the inner law is similar to that in the wake of a bluff body; for example, the wake function can be represented adequately by $2\sin^2[(\pi/2)(y/\delta)]$, which is reminiscent of the wake profile. (For this reason, the outer part of the boundary layer is called the wake region.) This observation emphasizes that the interaction between the turbulent flow and the free stream is similar to that in wakes and, by inference, in other free shear flows.

Such a similarity is reflected, among other things, by the so-called outer layer intermittency. A point probe located in the outer layer is sometimes in the turbulent region and sometimes outside of it, and therefore shows a roughly on-off characteristic (Corrsin & Kistler 1955). The simplest characterization of this intermittent behavior is the so-called intermittency factor (Townsend 1947), which is merely the average time spent by a point probe in the turbulent region. The intermittency factor varies with the distance from the wall, being unity nearly all the way in the constant stress region, decreasing further outwards roughly as an error function – a feature shared by all commonly studied free-shear flows. Much of this type of work beginning with Corrsin & Kistler (see also Klebanoff 1955) perceived that a sharp contiguous interface separates the turbulent regions from the non-turbulent ones. Later, the notion of such an interface was incorporated (for example, by Kovasznay, Kibens & Blackwelder 1970) into special forms of conditional measurements such as averages in the turbulent and non-turbulent zones, as well as the 'fronts' and 'backs' of the interface. Measurements of the same type in wakes (Thomas 1973) as well as other free shear flows support this similarity.

Similar interfaces are thought to exist for scalar quantities such as temperature in a heated boundary layer, or for a dye injected upstream in a liquid flow. Although turbulence does spread the scalar very effectively, there is no reason to expect that a scalar interface will in general be the same as the vorticity interface.

Now we know from visualization by optical techniques of thin sections of the flow and subsequent image processing that such interfaces are far more fragmented (see, for example, Prasad & Sreenivasan 1989), and probably not even contiguous, and is reasonably well represented by a fractal-like entity (Sreenivasan & Meneveau 1986); it takes a contiguous form essentially when some coarse-graining is applied. (We do not imply that large structures are absent; see section 2.6 and 3.3). Unlike mathematical fractals (Mandelbrot 1982) where scale-similarity extends over an infinite range of scales, the self-similar scale range is bounded here on both sides: The outer cut-off is of the same order as the boundary layer thickness, while the inner cut-off is on the order of the Kolmogorov scale. Incorporating this notion of cut-offs, ideas have been advanced (Sreenivasan, Ramshankar & Meneveau 1988) for successfully calculating the scaling laws for the mixing and entrainment of the ambient fluid into the turbulent region.

Outer layer intermittency in vorticity fluctuations is not possible in pipe and channel flows. This does not necessarily preclude a thermal interface between boundary layers if one of the walls of a channel gets heated, but we do not know of any such experiments.

2.6. A first approximation to interaction dynamics: We have already noted that a potentially useful point of view to take in explaining the boundary layer dynamics is to consider the wall as a sink of momentum, and that the inward flux of momentum governs the boundary layer dynamics to a first approximation; we further assume that only neighboring fluid layers interact, and that distant

layers of fluid, for example a fluid layer in the viscous region and another in the outer region, do not interact directly. This 'local momentum transfer theory' also neglects possible 'intermittency effects' concerning large variability in space and time of quantities of primary interest such as the turbulent shear stress. As already remarked, this description of the boundary layer dynamics is analogous to Kolmogorov's (1941) theory of local energy transfer across wave number space, ignoring both non-local and intermittency effects. Spectral theory in turbulence research has since been embroiled over questions of whether this picture is correct, and a similar line of enquiry (although in a different guise, see below and section 4) has been much on the horizons of research in turbulent boundarys layers also.

Before we criticize, modify or discard this point of view, it is useful to remind ourselves of its success, paralleling the similar success in the Kolmogorov-type spectral theories. It predicts that the inner layer dynamics is of the quasi-equilibrium type, governed entirely by the parameters ν, τ_w and y; in the equilibrium layer, ν becomes irrelevant, predicting the log-law, the -1 power law in spectral space, etc. These predictions have been verified amply by experiments. Although intermittency effects can be included, it is not clear that they will be profound.

In this view, the inward momentum flux constitutes a hierarchical 'momentum cascade' process. Recall that although the Kolmogorov energy cascade proceeds on the average from the low wave number to the high, there is no restriction that the energy flux cannot reverse its direction instantaneously. In a similar fashion, momentum can flow from the wall region to the outside region locally in time and space. In contrast to Kolmogorov's theory in which the significance of the anticascade of energy is unclear, the analogous anticascade here should clearly be important. The experiments of Uzkan & Reynolds (1967) seem to suggest that the wall plays a greater role than being merely a sink of momentum; the precise role of the wall is not fully understood, however, and we can only attempt a roughly self-consistent description.

Lighthill (1963) argued that the main effect of a solid surface on the incoming turbulent vorticity is to stretch it in the spanwise direction, and briefly set forth the basis for his arguments. Even though some caution is in order because vortex stretching is not the only possible nonlinear action possible (as can be seen from the equations for the mean square vorticity), such arguments are of some value. This can be seen from the fluctuating velocity and vorticity data (section 2.1) which show that the largest vorticity component is indeed in the spanwise direction; measurements of Blackwelder & Eckelmann (1979) also support Lighthill's picture. That the stretching is primarily in the spanwise direction (although streamwise stretching no doubt plays a part) is consistent with the observation that the principal effect of increasing only the streamwise stretching (as in highly accelerating boundary layers) is to kill turbulence rather than enhance it. The inward flux of momentum must accompany the stretching effect which gets stronger as one nears the wall until, in the buffer layer, the viscous effects balance the nonlinear stretching.

One can obtain a feel for near-wall vorticity generation by measurements of the skewness of the velocity derivative. In homogeneous and isotropic turbulence, this quantity signifies the inertial transfer of energy across the wave number domain; it is also proportional to the production of mean square vorticity by stretching. Both these effects are due to the nonlinearity of the equations of motion. It is not clear if these interpretations hold for the wall-bound anisotropic turbulence, but we shall assume that it is valid in a qualitative sense. There are no data on the skewness of the space

derivative of velocity fluctuations, but comparable data on the time derivative do exist. Although, because of the high shear near the wall, converting time to space by invoking Taylor's frozen flow hypothesis is questionable, the expectation is again that qualitative interpretations will be possible.

The derivative skewness measurements have been made, among others, by Comte-Bellot (1963, channel), Ueda & Hinze (1975, boundary layer), and Elena & Dumas (1978, pipe flow). Data from Elena & Dumas shown in figure 22 are representative, and suggest that the derivative skewness peaks at around $y^+ = 12$ where it is of order unity, and drops off to both sides. The value in the fully turbulent region is on the order of 0.4, not very different from the usual value in isotropic and homogeneous turbulence. The behavior closer to the wall is somewhat different in different experiments, but the collective evidence seems to favor the view that it drops off to zero at the wall. Whatever the details, it seems clear that the nonlinear effects are prominent around $y^+ = 12$, and more effective in that vicinity than elsewhere.

Lighthill viewed that most of the vorticity fluctuations thus generated constantly battle against turbulent and viscous diffusion, but that some of it will escape outwards. This escaped vorticity is facilitated in its upward mobility by the v-fluctuation, itself generated by the stretching action. This, in turn, is responsible for entraining the outer inviscid fluid, which begins its long route towards replenishing the lost momentum at the wall. The story is, in some sense, thought to be complete.

While this view explains some observed features, it does not account for two important aspects. First, the *energy containing motion* in the constant-stress region is independent of the details of the viscous region; as pointed out already, these aspects in the log-region of the atmospheric surface layer above the ocean are not different from those in the smooth-wall boundary layer. Second, this does not explain the observed structural features – that is, those aspects of the motion which can be given some identity either in visual or probe measurements. The sense that there is more to the boundary layer dynamics is motivated by flow visualization observations which call to question the basic premise of local interactions. One thought, for example, is that bursts occurring in the buffer layer travel far into the logarithmic region, and, if low-Reynolds number experiments are any guide, also into the outer region. Another thought is that the outer layer large eddies promote nonlocal interactions. It is possible that our visual perception is burdened by low-Reynolds number experience, and detailed experiments at high Reynolds numbers are therefore expected with much eagerness. It may well be that no new structures are likely to arise at high Reynolds numbers, but their interaction and relative importance is almost certain to undergo a change. Although high Reynolds number experiments have profound experimental difficulties, it is clear that dynamical views based exclusively on structural observations at low Reynolds numbers must be tempered by caution. It is useful to remind ourselves that an important aspect of the turbulent boundary layer, namely the separation of the inner and outer scales, does not obtain at low Reynolds numbers, and that any physical picture derived only from low Reynolds number measurements must be examined for consistency with asymptotic arguments mentioned already at different places.

3. The structural elements

Experiments have identified a multiplicity of structural elements, and the first comprehensive compilation is now being made by Robinson & Kline (1988). The value of the 'structure work',

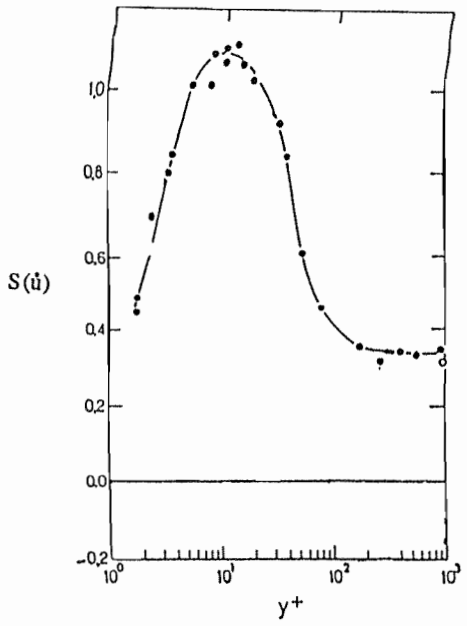

Figure 22. The skewness of the velocity derivative du/dt in the inner region of a pipe flow. Data from Elena & Dumas (1978).

which inquires into the mechanisms of various transport processes occurring in the boundary layer, cannot be overemphasized, especially in the context of boundary layer control.

A significant part of the early work relied heavily on measurements at a single point or a few small number of points in the flow. From appropriate correlation measurements, deductions about 'average' turbulent eddies were made (Townsend 1956, 1976, Grant 1956, Tritton 1967); note must also be made of the outer layer intermittency measurements of Corrsin & Kistler (1955) which brought forth the notion of an outer layer large eddy. The space-time correlation measurements (Favre et al. 1957, Willmarth & Wooldridge 1962, Kovasznay et al. 1970, to name but a few) have been especially valuable. Later work has emphasized flow visualization work, and an example of how it can be incorporated as an integral tool of quantitative point measurements can be found in Falco (1977, 1983). Low Reynolds number flows have now been simulated directly on supercomputers without invoking any specific turbulence models (Moin & Kim 1982, Spalart 1987); from these data bases one can deduce many flow features normally inaccessible to measurement. A number of kinematic details have been extracted already (e.g., Kim 1983, Brausser & Lee 1987, Robinson & Kline 1988), and it is clear that rapid advances in this direction will continue to be made. Our efforts here are better spent on the dynamical interpretation of some generic aspects. A useful complementary reference is Cantwell (1981).

3.1. The viscous region: The evidence appears incontrovertible (Kline et al. 1967) that a streaky structure in the velocity distribution near the wall is an ubiquitous feature of the turbulent boundary layer, at least at low Reynolds numbers; see figure 23. (In this figure one is looking down into the flow, and the flow is from top to bottom.) The streaks pervade the entire viscous region, but seem most pronounced around a y^+ of 9. They bear some resemblance to Townsend's (1956) countercurrent attached eddies, but details are quite different. The streaks occur randomly in space and time, but any given realization preserves definite spatial coherence. One significant conclusion of the work of Kline et al. concerns the average spanwise spacing of streaks. Figure 24 shows the collection of all the data available on the spanwise spacing $\Lambda^+ = \Lambda U^*/\nu$ of the streaks. There is no discernible trend with Reynolds number, and the mean spacing of around 100 wall units, borne out by nearly all subsequent investigators, is remarkably close to the early values given by Kline et al. Further measurements have refined the specifics of this picture. The sublayer streaks are believed to be of the order of 1000 wall units long (Blackwelder 1978, Praturi & Brodkey 1978, Blackwelder & Eckelmann 1979), but the vortical structures associated with them are more like a tenth as long (Kim 1983): The streaks, being the product of the accumulated dye, hydrogen bubble or other markers, are longer. They are centered at about 10 wall units from the wall (e.g., Blackwelder & Eckelmann 1978).

The streaks are believed to be significant because they form the precursor to the so-called bursting event (figure 25). As more and more observations have become available, refinements of the definition of bursting have been introduced; however, the essence is contained in Kline's (1978) proposal: It consists of a sequence of quasiperiodic events comprising of the formation of streaks, their lift-up, oscillation and breakdown. The bursting event itself is perceived to be significant because it presents a possible scenario for the interaction between the inner and outer regions of the flow; further, it is believed to be responsible for a significant fraction of the turbulent energy

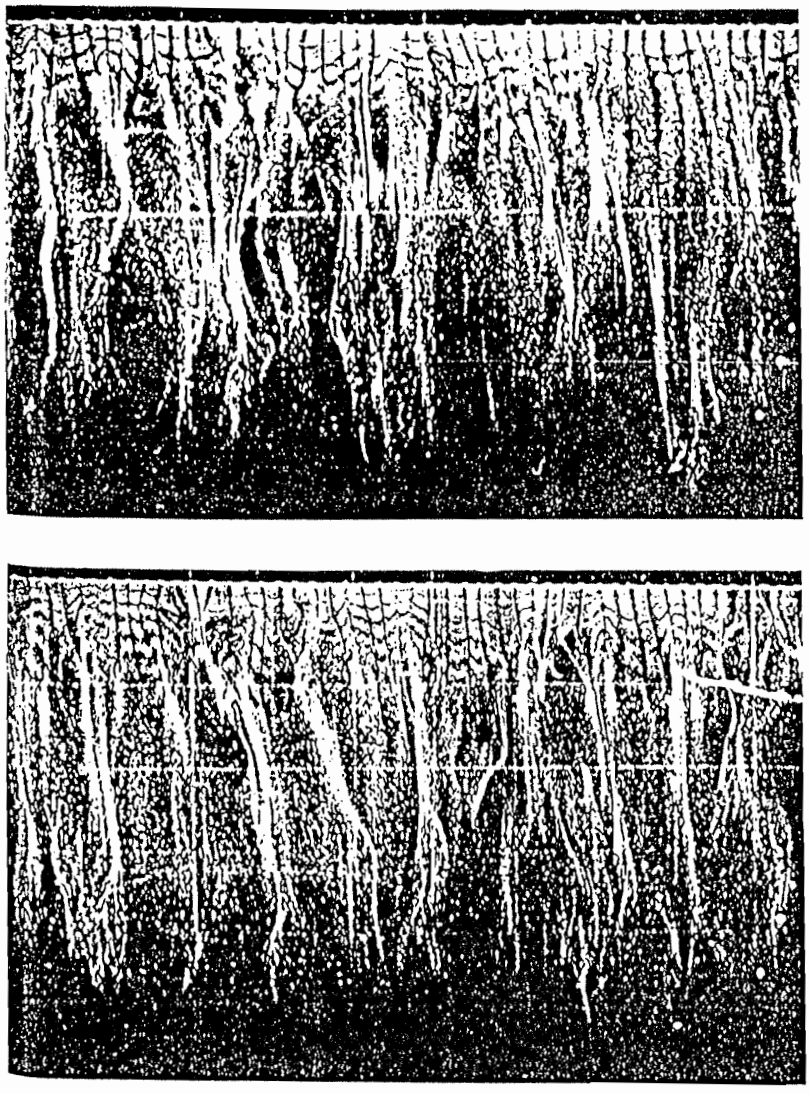

Figure 23. Photographs showing the accumulation of hydrogen bubbles in the form of streaky structures in the wall region of the boundary layer. Pictures from Kline et al. (1967).

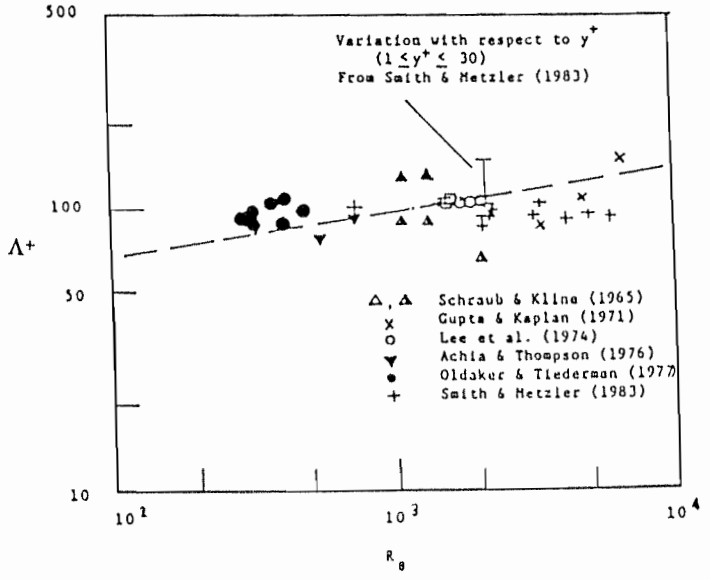

Figure 24. The spanwise spacing of streaks, normalized by wall variables. All measurements are in the viscous region, but measurement techniques differ from one author to another. The line drawn through the data will be explained in section 3.3. From Sreenivasan (1987).

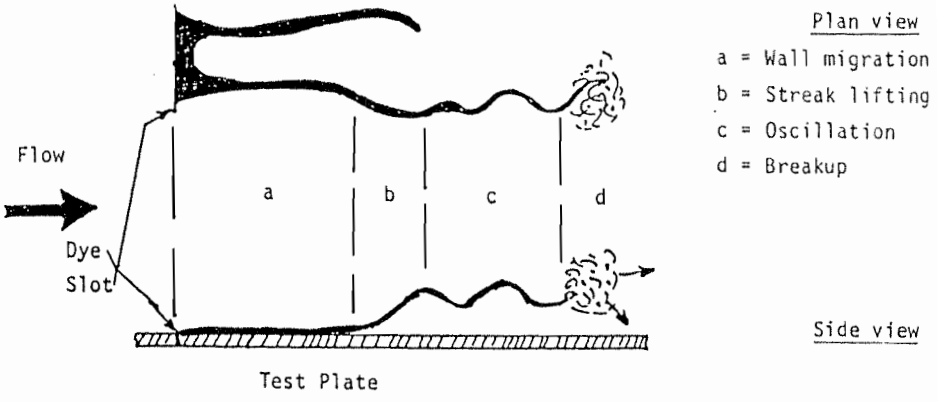

Figure 25. Schematic view of the near-wall bursting as seen by dye injection through the wall, from Kline (1978).

production (Kim, Kline & Reynolds 1971, later elaborated also by Wallace, Eckelmann & Brodkey 1972). In the experiments of Kline et al. (1967) the streaks of hydrogen bubbles drifted away from the wall as they move slowly, corresponding essentially to viscous diffusion effects. When a streak reaches a y^+ of about 10, it begins to oscillate and, upon reaching sufficient amplification, terminates in an abrupt break-up in the buffer region. These experiments showed that hydrogen bubbles after the break-up move along in a trajectory at least up to the lower portion of the log-region. To this picture, Corino & Brodkey (1969) added the so-called sweep event consisting of the streamwise movement of the upstream fluid sweeping away the previously ejected fluid – an event essentially demanded by continuity. The notion is that the sweep stabilizes the wall region, until a new cycle of these same events repeats. Other suggestions include pockets and ring vortices (Falco 1987).

Although remarkable amount of information is now available about streaks – only gross details have been presented here – their importance in the interaction dynamics remains unclear. In an interesting set of experiments, Grass (1971) has shown that the nature of interaction between the inner and outer regions remains quite similar whether the wall is smooth or covered with roughness elements protruding up to about 80 wall units, well outside the viscous region. This may be interpreted as minimizing the importance of streaks. On the other hand, smooth-wall data in drag reduction by polymer addition (e.g., Donohue, Tiederman & Reischman 1972, Oldaker & Tiederman 1977, Tiederman, Luchik & Bogard 1985) or by stable stratification (e.g., Kasagi & Hirata 1976) show that there is a direct correlation between increased streak spacing and skin friction reduction.

Even if it were true that streaks play a lesser role than has often been believed, a proper explanation for their existence has remained a challenge. The earliest explanation due to Kline et al. followed Lighthill's (1963) suggestion that a spanwise variation of the streamwise velocity will result when the stretched vortex elements in the viscous layer relax and contract. Another simple explanation (Acarlar & Smith 1987a, b) is that they mark the tracks of the haippin eddies in the outer layer (see later) that are being dragged along. Coles (1978) and, following him, Brown & Thomas (1977) have tried to explain them by invoking some kind of centrifugal instability of the viscous layer, it being generated when a 'big eddy' (which is two-dimensional on the scale of the streak spacing) from the outer layer passes over the sublayer region. The notion is essentially that when the big eddy moves with a convection velocity different from the local velocity, the particle paths underneath assume a curvature that is concave upwards – leading to the Görtler instability. For the notion to be useful, it is necessary to show that, among a host of other possible instabilities, it is indeed the Görtler kind that dominates; it should also be shown that the Görtler number exceeds the critical value substantially, and that the corresponding growth rates are large enough for the perturbations to grow to saturation amplitudes before encountering regions of convex curvature – which also occur on either side of the concave one. The situation is hopeless in a strict sense, but some plausible details were filled in by Sreenivasan (1987), who noted that the eddies driving the centrifugal instability were not of the boundary layer scale, but of the intermediate scale equal to the geometric mean of the inner and outer scales. His estimate for the streak spacing was in close agreement with the experimental data of figure 24. Yet another explanation is due to Phillips (1988) who proposed that they are merely a result of the back effect of the oscillatory disturbances on the mean flow.

If the primary effect of the wall is to produce a large magnitude of shear, it is reasonable to examine whether the uniform shear of the right magnitude can account for the observed streaky structure. The numerical simulations of Lee, Kim & Moin (1987) seem to favor this view, although, to see the right structure, Lee et al. had to use a substantially larger shear than is found experimentally. They also tried to explain their numerical results by means of the rapid distortion theory. But, as we saw in section 2.6 (see also section 4.2), the largest nonlinear effects in the boundary layer are to be found in exactly the region where the rapid distortion calculations were being made, and so the qualitative correspondence between observations and rapid distortion results must be considered tentative. It is a correct but impotent conclusion that completely satisfactory explanation is yet to emerge.

There is nontrivial difficulty in quantifying the bursting event by probe measurements, even though, at least at low Reynolds numbers, it appears to be well-defined visually. One of the most controversial results concerns the mean period of the bursting event. Part of the problem in measuring this quantity is that bursting occurs randomly in space and time, and a few point probes would be unable to determine their occurrence unambiguously. A fuller discussion can be found in Offen & Kline (1974) and Bogart & Tiederman (1986,1987). Earlier conclusions of Kline et al. (1967), substantiated by several follow-up studies (for example, Blackwelder & Haritonidis 1983), is that the appropriate scaling is on wall variables. This is a natural conclusion consistent with the notion that wall phenomena are governed by wall variables. Interest surged when, on the basis of hot-wire measurements around the edge of the viscous layer, Rao, Narasimha & Badri Narayanan (1971) concluded that the mean period $\langle T \rangle$ between bursts scaled on the outer variables U_o and δ, and that $U_0\langle T \rangle/\delta$ is about 5. There is evidence in favor of this observation also (Laufer & Badri Narayanan 1971, Willmarth & Lu 1972, Blackwelder & Kaplan 1976). Bandyopadhayay (1982) examined all the available data, and concluded that neither the inner scaling nor the outer scaling explains all observations. Mixed scaling consisting of the geometric mean of the inner and outer scales has also been proposed (Johansson & Alfredsson 1982). There is some approximate rational basis for expecting this scaling to work (Sreenivasan 1986 – see also section 3.5).

It is difficult to see how a frequently occurring event in the viscous layer can be controlled by the boundary layer thickness, but it is not hard to rationalize that some rare event can in fact be so. We also note that even some gross characteristics of the boundary layer (see section 2.5) show some Reynolds number dependence at least up to R_θ of the order of 6000, and there are very few clean experiments at higher Reynolds numbers. The concept of incomplete similarity introduced in section 2.4 can be invoked to support the notion that an inner layer event should scale on outer layer variables (see Barenblatt 1979), but a more likely parameter on which incomplete similarity may occur is y^+ itself: Except below a y^+ of about 5, there is no reason to think that the only controlling parameters are ν and U^* (see section 2.3). A study of the details of measurements, not merely of the final results reported in publications, suggests that an equally likely explanation for the conflicting measurements is that different authors were in fact measuring different facets of the same event, or even different events altogether. This, however, is not the place for further elaboration of this controversial point.

3.2. The outer layer: Some evidence has been put forth (Townsend 1966; Kovasznay et al. 1970) to suggest that the outer structure of the boundary layer is domimated by the so-called large eddies of size comparable to δ. Kovasznay et al. (1970) determined that these bulges are of the order of 3δ in the streamwise direction, and δ in the spanwise direction. They conjectured that the large eddies are passive so that new turbulence originating in the wall region is responsible for producing the Reynolds stress, and that the bursting initiates a process that eventually leads to the above large scale structure. Kovasznay (1970) speculated that 'bursting' of some kind occurs at all intermediate scales, and that the large structure is the culmination of a sequence of amalgamations occurring in the constant stress region (see also Offen & Kline 1974). On the other hand, Head & Bandyopadhyay (1981) suggest that the large eddy apparent in flow visualization studies is only the slow overturning motion of a collection of smaller scale eddies of the hairpin type, each of which is inclined, over a major part of the thickness, at around 45^{o} to the plane of the flat plate (see figure 26). Among other things, they emphasize that hairpin structure is found unambiguously only for $R_\theta > 7000$, and that it is Reynolds number dependent below this R_θ and so untypical. Their hairpin structures are similar to those hypothesized many years ago by Theodorsen (1955). One of their claims is also that Falco's (1977) typical eddies are tips of the hairpin eddies. Motivated by these observations, Perry & Chong (1982) and Perry, Henbest & Chong (1986) hypothesized that the essential structure of the outer flow is a hierarchy of hairpin eddies, and proposed a model for the near-wall dynamics on that basis.

Other structural elements such as the double roller-type eddies have also been identified (Townsend 1956, Kim & Moin 1986, Nagib & Guezennec 1986). This structure has been deduced in the latter two papers from conditionally averaged measurements (although the details of the conditional averaging are different in the two cases). The primary conclusion is that this structure has a characteristic length of the order δ in the streamwise direction, and is responsible (see Nagib, Naguib & Wark 1988) for the production of the Reynolds stress – even though it is quite weak. A possible dynamical explanation for the appearance of this structure was given by Sreenivasan (1987). Earlier, Praturi & Brodkey (1978) had identified the so-called transverse structure, which they linked to outer layer bulges as well as wall layer dynamics. In spite of the similarity to the double roller structure, the scales in the latter two cases appear to be different.

3.3. The inner-outer interactions: It is clear that the boundary layer structure is many-faceted and complex. In describing them, we have clearly not done full justice to every aspect discussed in the literature, partly because some of these structural elements are not independent, and partly because we do not understand where they all fit into the broader scheme of things. Even so, we are left with a number of them, and the puzzle is to decide which among them are dynamically significant, and how they arise and interact. If, for the sake of the argument, we assume that the large structure is indeed the dominant and driving mechanism, the question arises as to how it originates and maintains itself. We can rule out laminar-turbulent transition as the source, because their occurrence has been noted in heavily tripped flows where the usual transition details have been bypassed. It is also not hard to argue that the bursting process is unlikely to accomplish this, merely on the basis that its scales and the large eddy are quite disparate at high Reynolds numbers; to our knowledge, no one has observed the hierarchical amalgamation of scales required to make the point

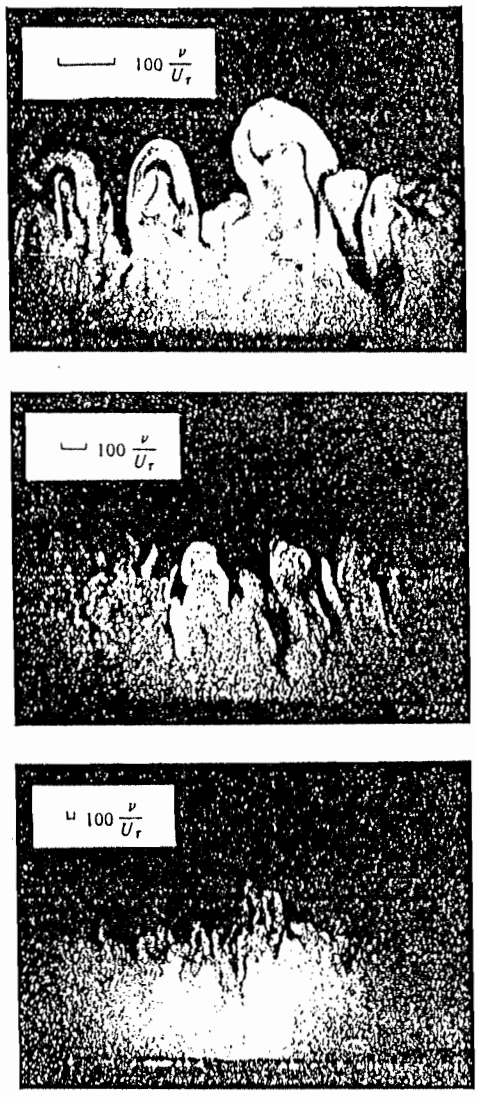

$R_0 = 600$

$R_0 = 1700$

$R_0 = 9400$

Figure 26. Sections of the boundary layer with 45° downstream plane illumination showing hairpin structures. Scales of ν/U^* are indicated. Picture from Haed & Bandyopadhyay (1981).

of view viable. Alternatively hypothesizing that bursting is the dominant aspect shifts our concern to *its* origin and sustained maintenance, and difficulties still remain. If we argue (e.g., Blackwelder 1978) that bursting arises purely from local instabilities in the viscous region, it is tantamount to saying, at high Reynolds numbers, that an extremely small fraction of the entire thickness (see figure 5) drives the rest of the flow having no active role – a sentiment that has been called to question. If we propose instead that bursting is driven by the outer structure (Rao et al. 1971), the nature of the inner/outer interaction has to be understood, and we are back to asking how the outer structure which drives the phenomenon came into being in the first place. If we take the view that the outer structure is of the hairpin-type (Theodorsen 1955, Head & Bandyopadhyay 1981, Wallace 1984, Lynn 1987), we are faced with difficulties in explaining their origin. The same can be said of the the origin of the double rollers and transverse structures. Few explanations in currency are quantitative and self-consistent – that is, almost no existing explanation satisfactorily accounts for each aspect of the boundary layer in relation to every other aspect.

One prevalent view is that many observed structures are the result of some kind of instability. It is useful to bring to focus the qualitative meaning, usually unspoken, of the deterministic stability calculations in explaining turbulence structure; for convenience, our discussion is focused on the large eddy. When all turbulence scales in the boundary layer are resolved, it is immediately clear, even at moderate Reynolds numbers, that a wide spectrum of scales is present, ranging from the Kolmogorov scale to a multiple of an integral scale. There is in turbulence theory a long-held belief (Richardson 1922) that these scales are statistically self-similar. Together, these two features lead to the expectation that the turbulence structure is fractal-like (Sreenivasan & Meneveau 1986); the value of this notion has now been demonstrated at least in some cases (e.g., Sreenivasan et al. 1988, Gouldin 1987). When some coarse graining is performed on these scales (either by instrument smoothing, conditional averaging, or some other means), one begins to perceive the large scale contiguous structures. The general belief is that the degree of coarse-graining beyond a certain point is not crucial to conclusions on the geometry and topology of the large structures. One may therefore view the large structure as the result of a judicious coarse-graining performed on the spatially and temporally resolved three dimensional flow field. An alternative point of view – whose basis is yet to be explored in detail, but whose usefulness becomes obvious as soon as it is stated – is that these large structures are the result of instability of a caricature flow which itself is the result of applying a suitable coarse-graining to the real flow. Whether the structures deduced by coarse graining the full solution are the same as those deduced by the instability of its caricature deserves a lot of thought but, if correct, the benefits of this notion are likely to be many.

As already remarked, Sreenivasan (1987) argued that the appropriate caricature of the turbulent boundary layer is a fat vortex sheet located at a distance from the wall given by (17), representing the location of the maximum Reynolds shear stress. It was shown that two and three dimensional instability, both inviscid and viscous, of this coarse-grained flow leads to an explanation for a number of observed features such as the double-roller structures, hairpin eddies, and the wall streaks; the line drawn through the data in figure 24 is from this theory. One of the primary conclusions of this analysis is that a dynamic reason exists for expecting energetic motions on the scale equal to the geometric mean of the inner and outer ones. One can infer that such scales have been seen in a number of experiments (Kline et al. 1967, Dinkelacker et al. 1977, Brown &

Thomas 1977, Falco 1977). Another interesting point is that the convection speed of these eddies, deduced by Sreenivasan, was $0.65U_0$, consistent with conclusions of the experimental work just cited. Further, the theory explains one of the peaks in the space-time correlation measurements of the wall pressure (Willmarth & Wooldridge 1962): Their correlation surface $R_{pp}(x,t)$ showed that pressure-producing small eddies travel at a speed of $0.69U_0$, quite close to $0.65U_0$ mentioned above.

It is worth emphasizing that in 'concentrating' all the mean flow vorticity in a fat 'sheet' of vorticity we are no longer concerned about the details of the mean velocity distribution; the implication is that the large-scale instabilities of the two are the same. It follows that one of the *a priori* requirements for the reasonableness of this approach is that the mean velocity distribution itself be unstable. This requirement is not necessarily satisfied by the boundary layer at the linear stage of instability, but the perturbation environment is in general *not* linear.

4. Some concluding remarks

We have presented a brief review of the turbulent boundary layer in some consistent way. It must be noted that the literature on the problem is so undauntingly large (and some of it is undigested) that it has not been possible to do justice to every paper on the subject, even all worthy ones. We have chosen to present what in our view constitute the essential aspects, sometimes at the expense of lacking elaborate references to fine details. We now discuss some isolated aspects deserving of further attention.

4.1 The role of direct numerical simulations and experiments: Much can now be computed, and the future looks even brighter because of the likely progress in computing technology, especially parallel architecture and special purpose machines. The power of such computations is that almost any quantity of interest can be extracted, many of them inaccessible to experimentalists in spite of the tremendous progress made in instrumentation in the last decade. Even so, it is clear that direct simulation of turbulent flow fields will be impossible at all but 'moderate' Reynolds numbers. Unfortunately, reasonable extrapolation of available experimental techniques based on laser diagnostics and other optical methods does not suggest that they can do much better.

An eventual goal of detailed scientific study is to build successful working models. By definition, even a highly successful model does not account for every detail, but two of its hallmarks are wide applicability and well-understood limitations. In this regard, a useful role of computations is that they should unravel the proper physics, which can then be used in modeling high Reynolds number flows. A useful role of experiments is that they should determine the proper scaling relations for the dynamically important events. Fortunately, useful scaling relations can be determined without requiring full three-dimensional flow field data, as long as we understand what we are measuring – say, with a single probe.

In computations as well as modern experiments dealing with turbulent phenomena, the crucial problem is often one of reducuing the massive bulk of data in ways that can be comprehended efficiently. Here, a lot of help is being offered by formal advances in nonlinear dynamics (e.g., Aubry, Holmes, Lumley & Stone 1988), proper orthogonal decomposition (e.g., Sirovich, Maxey & Tarman 1988), multifractals (e.g., Meneveau & Sreenivasan 1987a) as well as graphical display

capabilities. Unfortunately, the information extracted to-date has largely been kinematic in nature. Kinematic description, however interesting, is only the beginning: One must graduate beyond merely showing that a complex phenomenon like turbulent boundary layer is indeed complex.

4.2. Linear modeling of the inner layer: It is often thought (e.g., Einstein & Li 1956, Hanratty 1956, Sternberg 1962, Landhal 1967, Schubert & Corcos 1967) that the viscous layer can be modeled by linear equations. While the details are different from one work to another in this list, the commonality among them justifies bunching them together, at least for present purposes.

The behavior of the ratio of a typical nonlinear term to the linear term is shown in figure 27. (In these computations, the linear term was estimated by the zero-crossing measurements of Sreenivasan, Prabhu & Narasimha 1983, and the nonlinear term was estimated by the measured stress gradients.) This suggests that strong nonlinearities are essentially confined to a narrow region centered around a y^+ of 15 or so (the precise value seems to depend marginally on the Reynolds number). This feature should be explored in the predictive modeling of the turbulent boundary layer, but we know of no such effort. One thought is that the rest of the boundary layer can be taken to be a linear problem driven essentially by strong random forcing in this region. The statistics of the random forcing must, of course, be provided by experiment. At around a y^+ of 15, the probability densities of all three velocity components are essentially symmetric but non-Gaussian. It is not clear, whether for present purposes, there is a need to consider these non-Gaussian effects.

4.3. The role of intermittent phenomena in turbulent boundary layers: It has long been felt that many important processes in turbulence are highly intermittent in nature. For example, the Reynolds shear stress (Willmarth & Lu 1972), the turbulent energy production (Kline et al. 1967), turbulent energy dissipation (Batchelor & Townsend 1949), etc. An extreme view would be that a small number of rarely occurring large amplitude events account for a major share of the dynamics. It is not clear if this is so, and needs to be quantified in detail. (If this is *not* true, the enormous emphasis in the recent turbulence literature on special and rare events is more or less misplaced.) At any rate, it is already clear that turbulence dynamics is not governed by Central Limit type statistics where a large number of marginally dissimilar events control the statistics. Such processes are best modeled by multiplicative processes in which some a simple dynamical step repeats over and over leading to the observed intermittency. This view has led to some remarkable success in modeling the energy cascade (Meneveau & Sreenivasan 1987b).

4.4. Non-canonical boundary layers: As remarked early in section 1, the study of the canonical case of the flat-plate smooth-wall boundary layer, we believe, will help us understand the boundary layer dynamics in the presence of other complex effects. On the other hand, there is some merit to the view that the study of the non-canonical boundary layers will help us understand the canonical case better. A case in point is the rough-wall boundary layer: By eliminating the viscous layer as we know it to be in the smooth-wall case, it can help us understand the role of the viscous layer. The Stratford boundary layer (Stratford 1959) in which the skin friction is zero is another example because it eliminates one of the driving forces in the turbulent boundary layer, namely the wall-ward momentum flux, and can therefore help us understand better its role. A study of pressure

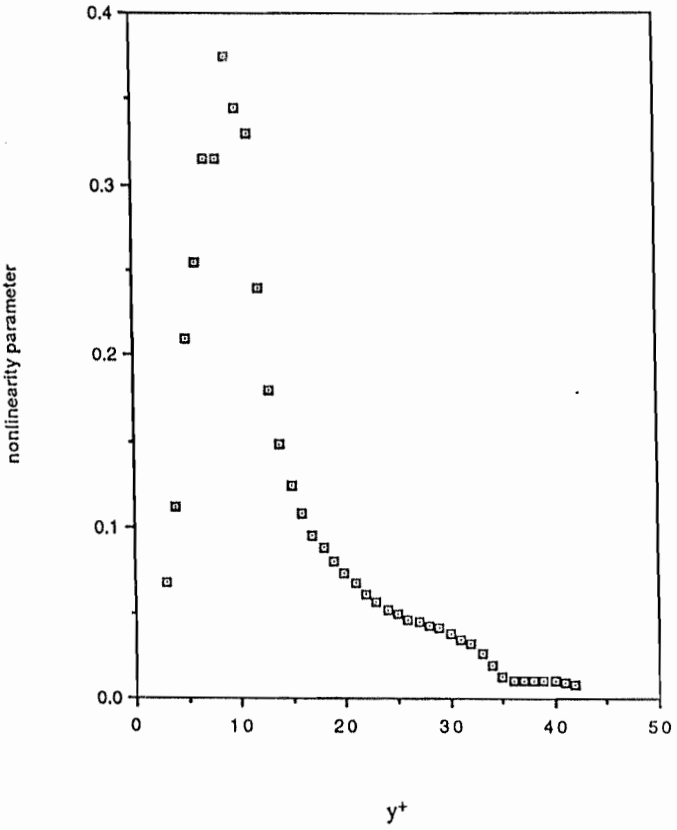

Figure 27. A typical ratio of the nonlinear to linear terms in the equations of motion computed in the viscous region.

gradient effects, curvature effects, compressibility effects, etc. can all be very helpful. The suggestion is not that data be generated to the same level of detail in all these non-canonical flows, but that some effort be devoted to them within a certain framework, with specific questions in mind.

Acknowledgements

This article would not have been written without the persistent efforts of Professor M. Gad-el-Hak, who constantly propped my flagging will by cajoling telephone calls and reminders. I have benefitted from discussions with a number of colleagues; to them, and particularly to B.-T. Chu, C. Meneveau, P. Kailasnath and K. Sreenivasan who commented on the draft, I am grateful. The work was supported by a grant from the Air Force Office of Scientific Reserach managed by Dr. James McMichael.

References

Acarlar, M.S. & Smith, C.R. 1987 J. Fluid Mech. **175**, 1.

Acarlar, M.S. & Smith, C.R. 1987 J. Fluid Mech. **175**, 43.

Achia, B.V. & Thompson, D.W. 1976 J. Fluid Mech. **81**, 439.

Andreopoulos,T., Durst, F., Zaric, Z. & Jovanic, J. 1984 Exp. in Fluids **2**, 7.

Aubry, N., Holmes, P., Lumley, J.L. & Stone, E. 1988 J. Fluid Mech. **192**, 115.

Badri Narayanan, M.A., Rajagopalan, S. & Narasimha, R. 1977 J. Fluid Mech. **80**, 237.

Batchelor, G.K. & Townsend, A.A. 1949 Proc. Roy. Soc. **199**, 238.

Blackwelder, R.F. 1978 In Lehigh Workshop on Coherent Structure in Turbulent Boundary Layers, ed. C.R. Smith & D.E. Abbot, p 211.

Blackwelder, R.F. & Eckelmann, H. 1979 J. Fluid Mech. **94**, 577.

Blackwelder, R.F. & Haritonodis, J.H. 1976 J. Fluid Mech. **132**, 87.

Blackwelder, R.F. & Kaplan, R.E. 1976 J. Fluid Mech. **107**, 89.

Bogard, D.G. & Tiederman, W.G. 1987 J. Fluid Mech. **162**, 389.

Bogard, D.G. & Tiederman, W.G. 1987 J. Fluid Mech. **179**, 1.

Bradshaw, P. 1967 J. Fluid Mech. **30**, 241.

Brausser, J.G. & Lee, M.J. 1987 NASA Rep. CTR-S87, p.165.

Bremhorst, K. & Walker, T.B. J. Fluid Mech. **61**, 173.

Brown, G.L. & Thomas, A. W. 1977 Phys. Fluids **20**, s243.

Cantwell, B.J. 1981 Ann. Rev. Fluid Mech. **13**, 457.

Clark, A.J. 1968 J. Basic Engg. **D90**, 455.

Coles, D.E. 1956 J. Fluid Mech. **1**, 191.

Coles, D.E. 1962 Rand Rep. R-403-PR.

Coles, D.E. 1978 In Lehigh Workshop on Coherent Structure in Turbulent Boundary Layers, ed. C.R. Smith & D.E. Abbot, p 462.

Comte-Bellot, G. 1963 Ph.D. Thesis, Univ. Grenoble. (Translated into English by P. Bradshaw as ARC31609, FM 4102, 1969.)

Corino, E.R. & Brodkey, R.S. 1969 J. Fluid Mech. **37**, 1.

Corrsin, S. & Kistler, A.L. 1955 NACA Tech. Rep. 1244.

Crocco, L. 1965 J. Soc. Ind. Appl. Math. **13**, 206.

Dinkelacker, A., Hessel, M., Meier, G. & Schewe, G. 1977 Phys. Fluids **20**, s216.

Donohue, G.L., Tiederman, W.G. & Reischman, M.M. 1972 J. Fluid Mech. **56**, 559.

Einstein, H.A. & Li, H. 1956 ASCE Proc. **82**, no. EM 2.

Elena, M. & Dumas, R. 1978 Paper 78-HT-4 presented at the ASME-AIAA Thermophysics & Heat Transfer Conference, Palo Alto, CA.

Falco, R.E. 1977 Phys. Fluids **20**, s124.

Falco, R.E. 1983 AIAA paper 83-0377.

Falco, R.E. 1987 Presentation at the Workshop on Turbulent Boundary Layer, Austin,Texas.

Favre, A.J., Gaviglio, J.J. & Dumas, R. 1957 J. Fluid Mech. **2**, 313.

Fortuna, G. & Hanratty, T.J. J. Fluid Mech. **53**, 575.

Gouldin, F. 1987 Rep. E-87-01 Cornell University; to appear in AIAA J.

Grant, H.L. 1958 J. Fluid Mech. **4**, 149.

Grass, A.J. 1971 J. Fluid Mech. **50**, 223.

Gupta, A.K & Kaplan, R.E. 1972 Phys. Fluids **15**, 981.

Gupta, A.K., Laufer, J. & Kaplan, R.E. 1971 J. Fluid Mech. **50**, 493.

Hanratty, T.J. 1956 AIChE J. **2**, 359.

Head, M.R. & Bandyopadhyay, P. 1981 J. Fluid Mech. **107**, 297.

Hussain, A.K.M.F. 1983 Phys. Fluids **26**, 2816.

Johansson, A.V. & Alfredsson, P.H. 1982 J. Fluid Mech. **122**, 295.

von Kármán, Th. 1930 Mechanische Ähnlichkeit und Turbulenz, Nachr. Ges. Wiss. Göttingen. Math. Phys. K1. p. 58.

Kasagi, M. & Hirata, N. 1976 In Proc. ICHMT Seminar on Turbulent Buoyant Convection

Kim, J. 1983 Phys. Fluids **26**, 2088.

Kim, J. & Moin, P. 1986 J. Fluid Mech. **162**, 339.

Kim, H.T., Kline, S.J. & Reynolds, W.C. 1971 J. Fluid Mech. **50**,133.

Klebanoff, P.S. 1954 NACA Rep. 1247.

Kline, S.J., Reynolds, W.C., Schraub, F.A. & Runstadler, P.W. 1967 J. Fluid Mech. **30**, 741.

Kline, S.J. 1978 In Lehigh Workshop on Coherent Structure in Turbulent Boundary Layers, ed. C.R. Smith & D.E. Abbot, p 1.

Kolmogorov, A.N. 1941 C.R. Acad. Sci. U.R.S.S. **30**, 301.

Kovasznay, L.S.G. 1970 Ann. Rev. Fluid Mech. **2**, 95.

Kovasznay, L.S.G., Kibens, V. & Blackwelder, R.F. 1970 J. Fluid Mech. **41**, 283.

Kreplin, H.-P. & Eckelmann, H. 1979 Phys. Fluids **22**, 1233.

Kudva, A.K. & Sesonske, A. 1972 Int. J. Heat Mass Tr. **15**, 127.

Landahl, M.T. 1967 J. Fluid Mech. **29**, 441.

Laufer, J. 1951 NACA Rep. 1053.

Laufer, J. 1954 NACA Rep. 1174.

Laufer, J. & Badri Narayanan, M.A. 1971 Phys. Fluids **14**, 182.

Lee, M.J., Kim, J. & Moin, P. 1987 In Sixth Symposium on Turbulent Shear Flows, Toulouse, Sept. 7-9.

Lee, M.K., Eckelman, L.D. & Hanratty, T.J. 1974 J. Fluid Mech. **66**, 17.

Lighthill, M.J. 1963 In Laminar Boundary Layers, ed. L. Rosenhead, Oxford University Press, p.48.

Long, R.R. & Chen, T-C. 1981 J. Fluid Mech. **105**, 19.

Lu, S.S. & Willmarth, W.W. 1973 J. Fluid Mech. **60**, 481.

Lynn, T.B. 1987 Ph. D. Thesis, Yale Univ.

Mandelbrot, B.B. 1982 The Fractal Geometry of Nature, W.H. Freeman.

Meneveau, C. & Sreenivasan, K.R. 1987a Nucl. Phys. B. (Proc. Suppl.) **2**, 49..

Meneveau, C. & Sreenivasan, K.R. 1987b Phys. Rev. Lett. **59**, 1424.

Millikan, C.B. 1939 In Proc. Fifth Cong. Appl. Mech. Cambridge, MA. p. 386.

Moin, P. & Kim, J. 1982 J. Fluid Mech. **118**, 341.

Monin, A.S. & Yaglom, A.M. 1971 Statistical Fluid Mech. vol. I, M.I.T. Press.

Nagib, H.M. & Guezennec, Y.G. 1986 Paper presented at the tenth Symp. on Turbulence, Univ. Missouri-Rolla.

Nagib, H.M., Naguib, A. & Wark, C. 1988 Bull. Amer. Phys. Soc. **33**, 2262 (abstract only).
Nakagawa, H. & Nezu, I. 1981 J. Fluid Mech. **104**, 1.
Nikuradse, J. 1932 Forsch. Arbeiten Ing.- Wesen, no. 356.
Offen, G.R. & Kline, S.J. 1974 J. Fluid Mech. **62**, 223.
Oldaker, D.K. & Tiederman, W.G. 1977 Phys. Fluids. **20**, s133.
Perry, A.E. & Chong, M.S. 1982 J. Fluid Mech. **67**, 257.
Perry, A.E. & Chong, M.S. 1982 J. Fluid Mech. **119**, 173.
Perry, A.E., Henbest, S. & Chong, M.S. 1986 J. Fluid Mech. **165**, 163.
Phillips, W.C.R. 1988 In Near-Wall Turbulence, ed. S.J. Kline, Hemisphere.
Pond, S., Smith, S.D., Hamblin, P.F. & Burling, R.W. 1966 J. Atmos. Sci. **23**, 376.
Prandtl, L. 1925 ZAMM **5**, 136.
Prasad, R.R. & Sreenivasan, K.R. 1989 Exp. in Fluids (in press).
Praturi, A.K. & Brodkey, R.S. 1978 J. Fluid Mech. **89**, 251.
Preston, J.H. 1958 J. Fluid Mech. **3**, 373.
Rao, K.N., Narasimha, R. & Badri Narayanan, M.A. 1971 J. Fluid Mech. **48**, 339.
Reynolds, O. 1894 Phil. Trans. Roy. Soc. Lond. **186**, 123.
Richardson, L.F. 1922 Weather Prediction by Numerical Process, Cambridge University Press.
Robinson, S. & Kline, S.J. 1988 In Near-Wall Turbulence, ed. S.J. Kline, Hemisphere.
Schildknecht, M., Miller, J.A. & Meir, G.E.A. 1979 J. Fluid Mech. **90**, 67.
Schraub, F.A. & Kline, S.J. 1965 Stanford Univ. Rep no. MD-12.
Sirovich, L., Maxey, M. & Tarman, H. 1987 In Sixth Symp.Turb.Shear Flow, Toulouse, p. 6-12.
Smith, C.R. & Metzler, S.P. 1983 J. Fluid Mech. **129**, 27.
Spalart, P. 1987 NASA TM 89407.
Sreenivasan, K.R. 1987 In Turbulence Management and Relaminarization, eds. H.W. Liepmann & R. Narasimha, Springer, p. 37.
Sreenivasan, K.R. & Antonia, R.A. 1977 J. Appl. Mech. **44**, 389.
Sreenivasan, K.R. & Meneveau, C. 1986 J. Fluid Mech. **173**, 357.
Sreenivasan, K.R., Prabhu, A. & Narasimha, R. 1983 J. Fluid Mech. **137**, 251.
Sreenivasan, K.R., Ramshankar, R. & Meneveau, C. 1988 Proc. Roy. Soc. Lond. (in press).
Sternberg, J. 1962 J. Fluid Mech. **13**, 241.
Stratford, B.S. 1959 J. Fluid Mech. **5**, 17.
Theodorsen, T. 1955 In 50 Jahre Grenzschichtforschung, ed. Goertler & Tollmien, Vieweg & Sohn
Thomas, R.M. J. Fluid Mech. **57**, 549.
Tennekes, H. & Lumley, J.L. 1972 A First Course in Turbulence, M.I.T. Press.
Tiederman, W.G., Luchik, T.S. & Bogard, D.G. 1985 J. Fluid Mech. **156**, 419.
Townsend, A.A. 1956 The Structure of Turbulent Shear Flow, Cambridge Univ. Press.
Townsend, A.A. 1961 J. Fluid Mech. **11**, 97.
Townsend, A.A. 1966 J. Fluid Mech. **26**, 689.
Townsend, A.A. 1976 The Structure of Turbulent Shear Flow, Cambridge Univ. Press, second ed.
Tritton, D.J. 1967 J. Fluid Mech. **28**, 439.

Ueda, H. & Hinze, J.O. 1975 J. Fluid Mech. **67**, 125.
Ueda, H. & Mizushina, T. 1977 In Proc. 5th Biennial Symp. on Turb. Univ.Missouri-Rolla.
Uzkan, T. & Reynolds, W.C. 1967 J. Fluid Mech. **28**, 803.
Wallace, J.M. 1982 In 11th Sotheast Conf. on Theo. and Appl. Mech. Huntsville, Alabama.
Wallace, J.M. 1986 Exp. Fluids. **4**, 61.
Wallace, J.M., Eckelmann, H. & Brodkey, R.S. 1972 J. Fluid Mech. **54**, 39.
Wieghardt, K. & Tillmann, W. 1951 NACA TM 1314.
Willmarth, W.W. & Bogar, T.J. 1977 Phys. Fluids **20**, s9.
Willmarth, W.W. & Lu, S.S. 1972 J. Fluid Mech. **55**, 65.
Willmarth, W.W. & Wooldridge, R. 1962 J. Fluid Mech. **14**, 187.